
Electronic Thesis and Dissertation Repository

6-27-2022 4:00 PM

Development of a Novel Rodent Model of Radiation-Induced Implant Capsular Contracture

Tanya DeLyzer, *The University of Western Ontario*

Supervisor: Turley, Eva, *The University of Western Ontario*

Co-Supervisor: Wong, Eugene, *The University of Western Ontario*

A thesis submitted in partial fulfillment of the requirements for the Master of Science degree in Surgery

© Tanya DeLyzer 2022

Follow this and additional works at: <https://ir.lib.uwo.ca/etd>



Part of the [Plastic Surgery Commons](#), and the [Radiation Medicine Commons](#)

Recommended Citation

DeLyzer, Tanya, "Development of a Novel Rodent Model of Radiation-Induced Implant Capsular Contracture" (2022). *Electronic Thesis and Dissertation Repository*. 8620.
<https://ir.lib.uwo.ca/etd/8620>

This Dissertation/Thesis is brought to you for free and open access by Scholarship@Western. It has been accepted for inclusion in Electronic Thesis and Dissertation Repository by an authorized administrator of Scholarship@Western. For more information, please contact wlsadmin@uwo.ca.

Abstract

Radiation-induced implant capsular contracture is a challenging complication of post-mastectomy breast reconstruction. The objective of this thesis was to establish a novel rodent model that replicates the critical properties of this complication. Retired breeder female Sprague-Dawley rats underwent surgery with custom smooth silicone implants placed under the right 4th mammary fat pad. Half these rats received 26Gy of ionizing radiation to the implant and fat pad. Radiated implants had both higher Baker grades of capsular contracture and Kumar scores denoting radiation-induced fibrosis. Irradiated capsules showed increased Masson's trichrome staining and significantly higher hydroxyproline to total protein ratio compared to controls, collectively indicating higher collagen levels in irradiated capsules. Picrosirius red staining qualitatively demonstrated a trend towards increased red birefringence in irradiated capsules, reflecting denser collagen bundling. This model is therefore a reliable reproduction of radiation-induced capsular contracture, and can be used to evaluate potential preventative and therapeutic non-surgical interventions.

Keywords

capsular contracture, implant capsular contracture, mammary fat pad, breast reconstruction, radiation fibrosis, rat model capsular contracture, collagen deposition, collagen fibril bundling

Summary for Lay Audience

Breast reconstruction can improve the quality of life for women with breast cancer. Reconstructing, or creating a new breast, with silicone implants is the most common technique. Excessive scarring around the implant is a difficult problem after surgery and is greatly increased when the patient has radiation treatment. This can be extremely painful and disfiguring for the patient. This thesis outlines the creation of an animal experimental model of this scarring around implants after radiation. For the study, 13 female rats had surgery to place implants below their breast tissue on the right side. Four weeks after surgery, half of the rats then received radiation treatment to the implant and breast tissue, the other half did not. The amount of scarring around the implants was examined and graded using known rating scales. The rats were sacrificed four weeks after radiation and eight weeks after surgery. The implant with surrounding scar and breast tissue were collected. Special tests were used to look at the scarring under the microscope and also to measure the amount of collagen in the scar around the implant. The difference between the rats receiving radiation and no radiation was compared. The radiation treatment created more scarring around the implant that could be seen and felt on exam. This could also be seen under the microscope with our special stains of the scar tissue. The radiated implant scar had more collagen measured with our special test. This thesis shows successful creation of an animal model of radiation created implant scar and has potential to impact the lives of women with breast cancer. This model is special because custom miniature implants were used that are exact copies of the ones used for patients. As well, the implants were placed below breast tissue which is unique, and replicates the position in patients. This model can be used in the future to further study this scarring and test possible medications that can prevent this problem.

Co-Authorship Statement

For Chapter 3 and 4: All of the laboratory experiments outlined were performed in Dr. Eva Turley's laboratory. The radiation experiments were performed under the supervision of Dr. Eugene Wong at the London Regional Cancer Program. Kathryn Minkhorst assisted with the animal experiments, as well as tissue histology and immunohistochemistry including the Masson's trichrome analysis and the tissue assays for hydroxyproline to total protein tissue assays. Ai Li Jia Li and Wei Cen Wang assisted with the picrosirius red analysis. Carl Postenka paraffinized, embedded, and sectioned all of the mammary fat pad specimens used in the analysis, as well as assisted with Masson's trichrome staining. Caroline O'Neil and Hao Yin from the Molecular Pathology Core Facility at Robarts Research Institute assisted with Picrosirius Red staining and performed the image acquisition.

Acknowledgements

I am extremely grateful for the opportunity to complete this thesis and be enrolled in the Master of Surgery program. I was met with many challenges in completing this thesis, but had many people that supported the completion this work. Firstly, I would like to acknowledge my supervisor, Dr. Eva Turley, for her continued guidance and encouragement. As well as Dr. Eugene Wong, whose knowledge and expertise with the radiation treatment was integral to the completion of this project.

To Kathryn Minkhorst, my Summer Research Training Program (SRTP) medical student, I am eternally grateful. Kathryn was integral to the completion of this project, assisting in organization of the animal experiments as well as the laboratory work. She has been invaluable.

Members of the Turley Lab (Conny Tolg and Violet Liu) - thank-you for your assistance and guidance. Again, Carl Potenska for tissue processing and Hao Yin for picosirius red imaging. Trisha Carter from Animal Facilities was especially helpful in ensuring success of the animal surgery and monitoring. My other medical students, Ai Li Jia Li (Erica) and Wei Cen Wang (Cathy) for their assistance with picosirius red analysis.

Justin Paulter and Habiba Sallem, students with Dr. Wong, assisted with radiation delivery. I am specifically thankful to Justin for his creativity and skill in designing and printing the 3D “ratform” used in Chapter 2 for radiation set-up.

Table of Contents

Abstract.....	i
Summary for Lay Audience.....	ii
Co-Authorship Statement.....	iii
Acknowledgements.....	iv
Table of Contents.....	v
List of Tables.....	vii
List of Figures.....	viii
List of Appendices.....	xi
1 Introduction.....	1
1.1 Breast Reconstruction.....	1
1.2 Post-Mastectomy Radiation Therapy.....	2
1.3 Breast Conserving Therapy.....	2
1.4 Breast Implant Capsular Contracture.....	3
1.5 Radiation Induced Fibrosis.....	4
1.6 Clinical Grading Scales.....	6
1.6.1 Capsular Contracture.....	6
1.6.2 Radiation Injury.....	6
1.7 Current Animal Models.....	7
2 Thesis Objective and Aims.....	11
3 Methods.....	12
3.1 Animal Experiments Overview.....	12
3.2 Surgery.....	14
3.3 Post-Operative Monitoring.....	16
3.4 Irradiation.....	16
3.5 Post-radiation Monitoring.....	20
3.6 Euthanasia and Tissue Harvest.....	20
3.7 Tissue Sectioning.....	22

3.8	Tissue Histology	22
3.8.1	<i>Hematoxylin and Eosin</i>	22
3.8.2	<i>Masson’s Trichrome</i>	23
3.8.3	<i>Picrosirius Red</i>	23
3.9	Tissue Assays - Hydroxyproline to Total Protein Assay	24
4	Results.....	26
4.1	Clinical Assessments	26
4.2	Masson’s Trichrome	30
4.3	Picrosirius Red	34
4.4	Tissue Assays - Hydroxyproline to Total Protein Assay	39
5	Discussion.....	41
5.1	Objective 1	41
5.1.1	<i>Aim 1</i>	41
5.1.2	<i>Aim 2</i>	42
5.1.3	<i>Aim 3</i>	43
5.1.4	<i>Conclusions and Limitations of Objective 1</i>	44
5.2	Objective 2.....	44
5.2.1	<i>Aim 1</i>	44
5.2.2	<i>Aim 2</i>	46
5.2.3	<i>Conclusions and Limitations of Objective 2</i>	46
6	Impact and Future Directions.....	48
6.1	Hyaluronan.....	48
	References.....	50
	Curriculum Vitae.....	57

List of Tables

Table 1. Baker Classification of Capsular Contracture after Augmentation Mammoplasty	6
Table 2. Kumar score and Baker grade for animals undergoing Surgery with Silicone Implant and Post-Operative Radiation to Right 4 th Mammary Fat Pad.	27

List of Figures

Figure 1. Animal Experiment Overview..... 13

Figure 2. Rat surgery set-up. Gas anesthesia provided via nose cone with 4th set of mammary fat pads clipped in preparation. 15

Figure 3. Intraoperative image of rat implant surgery demonstrating the pocket created below the right 4th mammary fat pad..... 15

Figure 4. “Mini” cohesive silicone gel implants supplied by Mentor/J&J. Base diameter is 2cm, and projection of the implants is 1cm. 16

Figure 5. First set of rats receiving radiation treatment were positioned in the induction chamber in the lateral decubitus position on a foam pad. The implant and fat pad isolated from the body using positioning sticks..... 18

Figure 6. The second set of rats receiving radiation treatment were positioned using a 3D printed platform “ratform” in the prone position within the induction chamber. 19

Figure 7. Side view demonstrating the implant and overlying fat pad falling through the platform to isolate away from the remainder of the body. The radiation beam was then directed from the horizontal position. 19

Figure 8. Demonstration of tissue harvest on right 4th mammary fat pad with implant and capsule en bloc. Dissection included fat pad from xiphoid cranially, extent of pad dorsal and ventral, and the caudal extent being the blood vessel to the 4th fat pad..... 21

Figure 9. Demonstration of left 4th mammary fat pad tissue harvest. The fat pad is demonstrated not yet harvested. The tissue harvest includes the yellow fat from xiphoid cranially to the blood vessel to 4th pad caudally, midline ventrally, and the dorsal extent of the fat pad. 22

Figure 10. Photographs of non-radiated rats at 8-weeks post-surgery with 4th right implant sub-mammary fat pad. Left 4th mammary fat pad sham surgery. All rats demonstrate a Baker Grade 1 capsule..... 28

Figure 11. Photographs of first set of rats at 4-weeks post-radiation treatment to the 4th right implant and mammary fat pad. Left 4th mammary fat pad sham surgery. All three animals demonstrate Baker Grade 2 firm capsules. 29

Figure 12. Photographs of second set of rats at 4-weeks post-radiation treatment to the 4th right implant and mammary fat pad using the 3D printed “ratform”. Left 4th mammary fat pad sham surgery. All animals demonstrate Baker Grade 3 capsules, and show persistent hair loss..... 29

Figure 13. Representative images of paraffin embedded tissue sections from non-radiated and radiated animals containing right 4th implant capsule and adjacent fat pad with architecture of the capsule preserved. Arrow points to capsule. A. H&E B. Masson’s Trichrome..... 31

Figure 14. Paraffin embedded tissue sections from non-radiated and radiated right 4th implant capsule and adjacent fat pad were stained with Masson’s Trichrome. Arrows denote capsule layer. Darker staining indicates greater collagen concentration. Two representative images each from one non-radiated and one radiated animal at 10X..... 32

Figure 15. Masson’s Trichrome image analysis using ImageJ software quantifying the mean greyscale (blue pixel density) in the right 4th implant capsule tissue and fat pad and left 4th sham surgery fat pad from radiated (n=7) and non-radiated animals (n=6), 6 ROIs per animal. 33

Figure 16. Masson’s Trichrome image analysis using ImageJ software quantifying the mean greyscale (blue pixel density) in the right 4th implant capsule tissue and fat pad from Set 1 radiated animals (n=3), Set 2 radiated animals (“ratform”, n=4), and non-radiated animals (n=6). 6 ROIs per animal. 34

Figure 17. Representative images of paraffin embedded tissue sections of right 4th implant capsule and adjacent fat pad stained with Picrosirius Red, at 10X. Red indicating denser collagen bundling and networks. A-C. Non-radiated. D-F Radiated. 35

Figure 18. Representative images of paraffin embedded tissue sections of right 4th implant capsule and adjacent fat pad stained with Picrosirius Red, at 40X. Red indicating denser collagen bundling and networks. A-C. Non-radiated. D-F Radiated. 36

Figure 19. Average red and blue pixel count for picosirius red 40X images of right 4th implant capsule and left 4th sham surgery fat pad for both radiated and non-radiated animals..... 38

Figure 20. Red and blue pixel count expressed as proportion of total pixel count. Picosirius red 40X images of right 4th implant capsule and left 4th sham surgery fat pad for both radiated and non-radiated animals..... 38

Figure 21. Calculated hydroxyproline (OHP) to total protein (tP) ratio for right 4th implant capsule and fat pad in radiated and non-radiated animals. Twenty-five 10uM sections from each animal were used (n = 7 radiated, n = 6 non-radiated). Six technical replicates were run per sample. 39

Figure 22. Calculated hydroxyproline (OHP) to total protein (tP) ratio for right 4th implant capsule and fat pad in radiated and non-radiated animals. Set 1 radiated animals (n = 3) and set 2 radiated animals using the “ratform” (n=4), twenty-five 10uM sections from each animal were used (n=6 non-radiated). Six technical replicates were run per sample. 40

Figure 23. Calculated hydroxyproline (OHP) to total protein (tP) ratio for the left 4th sham surgery fat pad in radiated and non-radiated animals. Twenty-five 10uM sections from two animals in both groups were used (2 non-radiated, 2 radiated). Six technical replicates were run per sample. 40

1 Introduction

1.1 Breast Reconstruction

In Canada, it was estimated that 27,400 women would be diagnosed with breast cancer in 2020¹. Due to increased screening and improvements in adjuvant therapies, the 2020 projected mortality rate was 22 per 100,000 population, a decline of 49% since its peak in 1986 (43 per 100,000 population)¹. The 5-year and 10-year survival rates for breast cancer are 88% and 82%, respectively². With improvement in overall survival, comes improvements in quality of life. One factor that can improve the quality of life of women with breast cancer is breast reconstruction. Women undergoing mastectomy can choose to have their breast reconstructed either using their own tissue (autologous) or with implants (alloplastic), and this is an informed decision that is made between the patient and surgeon.

Alloplastic, or implant-based breast reconstruction, continues to increase in popularity and remains the most common form of breast reconstruction³. Improvements in implants and techniques such as use of acellular dermal matrix, fat grafting, and nipple-sparing mastectomy have contributed to this increase in popularity as outcomes have correspondingly improved. In addition, there has been an increase in bilateral reconstructions as more women with breast cancer genes are identified and undergo prophylactic mastectomies⁴. In post-mastectomy implant-based reconstruction, a breast implant is placed either at the time of mastectomy (immediate reconstruction), or in a delayed fashion, after mastectomy and adjuvant therapies. If placed immediately at the time of mastectomy in a single-stage, the implant is most commonly placed below the pectoralis major muscle and acellular dermal matrix is used as a biologic mesh to support the implant. Increasingly, sub-glandular (pre-pectoral) reconstruction is being used in conjunction with acellular dermal matrix⁵.

In a delayed setting, a 2-stage procedure is required. First a temporary tissue expander is placed, and then after expansion has occurred, it is exchanged for a permanent implant. If adjuvant radiation has been given, then the tissue expander is most often placed in combination with autologous tissue by use of a latissimus dorsi pedicled flap. This is done for the purpose of bringing into the area non-radiated, and well-vascularized, tissue to allow for better expansion.

The most common autologous reconstruction option remains the DIEP flap (deep inferior epigastric perforator). This is a skin and subcutaneous tissue flap taken from the lower abdomen, that is transferred by microsurgical techniques to build the new breast.

1.2 Post-Mastectomy Radiation Therapy

According to the American Society of Clinical Oncology guidelines, indications for post-mastectomy radiation therapy (PMRT) include close (<4mm) or positive margins, large primary breast tumours >5cm, or 4 or more positive lymph nodes⁶. There are more recent guidelines however that suggest PMRT be considered in order to reduce locoregional recurrence in those with 1 to 3 positive lymph nodes^{7,8}. Post-mastectomy radiation therapy has been shown to reduce the rate of loco-regional recurrence in node-positive patients⁹. In the setting of expected adjuvant PMRT, immediate autologous reconstruction (DIEP flap) is often the preferred technique. This is because patients who have undergone immediate alloplastic breast reconstruction and require PMRT have been found to have poorer aesthetics scores, higher complication rates, including capsular contracture and reconstructive failure, and lower patient satisfaction scores in comparison to patients who do not receive radiation¹⁰. However, there may be reasons autologous reconstruction may not be an option for patients including; inadequate abdominal adipose tissue, prior abdominoplasty, or medical comorbidities prohibiting long anesthetics¹¹. In these cases, patients may decide on immediate alloplastic reconstruction even knowing the risks of radiation, as opposed to living without a breast. There are also instances where PMRT is not expected preoperatively, but then the final pathology dictates otherwise. In the setting of immediate alloplastic breast reconstruction, the rate of PMRT in the literature ranges from 15.9% to 17.0%^{6,12}.

1.3 Breast Conserving Therapy

In patients that undergo lumpectomy and breast conserving therapy (BCT), radiation therapy to the remaining breast has been shown to halve the rate of local recurrence¹³. In BCT patients, there can be loss of volume of the breast, creating asymmetry with the contralateral natural breast. In this setting, some patients seek out augmentation of the smaller breast in lieu of a reduction of the contralateral breast. In addition, there are patients that have previously undergone cosmetic augmentation and then subsequently develop breast cancer. Patients may be

candidates for BCT, and receive radiation therapy with their breast implant in situ. In each of these scenarios, there is the potential for a breast implant to be in the field of radiation during treatment, or subsequently being placed in breast tissue that has undergone radiation fibrosis. Breast augmentation remains one of the top 5 most common surgical cosmetic procedures according to the American Society of Plastic Surgery¹⁴. As the population ages, there will be increasing numbers of women who develop breast cancer with prior augmentation. A recent literature review showed that the risk of developing capsular contracture with BCT was 22%, with the risk being greater for whole breast irradiation and higher doses, compared to accelerated partial breast irradiation¹⁵. Current National Comprehensive Cancer Network (NCCN) guidelines recommend dosing regimens of 46-50 Gy in 23-25 fractions, or 40-42.5 Gy in 15-16 fractions for whole breast radiation. Typical boost doses, recommended in patients at higher risk for recurrence, relevant for patients who undergo BCT, are 10-16 Gy in 4 to 8 fractions¹⁶. Accelerated partial breast irradiation is reserved for select patients with low risk cancers.

1.4 Breast Implant Capsular Contracture

Breast implant capsular contracture is a difficult and unpredictable complication occurring in up to 25% of all implant based breast reconstructions¹⁷⁻²⁰. For women with breast cancer, adjuvant radiation therapy can improve long term survival rates and decrease local cancer recurrence, but also dramatically increases the rate of capsular contracture - up to 73%²¹. Normal capsule formation is the result of an inflammatory foreign-body response to the implant in order to promote wound healing and is necessary to produce a stable collagen capsule that maintains the implant position. Capsular contracture occurs if the response persists towards chronic inflammation, with persistent recruitment and activation of fibroblasts that differentiate into myofibroblasts, and thus leading to excessive myofibroblast activity that results in collagen deposition and bundling. This in turn causes fibrosis and contracture of a rigid collagen capsule^{22,23}. Activated fibroblasts and myofibroblasts are characterized by high expression of fibroblast activation protein (gene name FAP) and α -smooth muscle actin (aSMA, gene name ACTA2) respectively²⁴⁻²⁶. The pathological switch that propels a 'healthy capsule' towards contracture formation remains incompletely characterized, and the etiopathology is likely multifactorial. Interestingly, post-radiation delay of implant-based reconstruction does not

eliminate the risk of capsular contracture, indicating a persistent level of radiation-induced fibroblast activation leading to fibrotic progression^{27,28}.

Clinically, patients can experience painful capsular contractures, breast disfigurement, psychological distress, and risk of reconstructive failure with implant loss. A variety of preventative intra-operative techniques are used to reduce the incidence of capsular contracture such as triple-antibiotic solutions or povidone-iodine irrigation to wash implants prior to insertion, and limiting direct handling of implants, which have shown efficacy²⁹⁻³¹.

Pharmacological therapies such as steroids and systemic leukotriene antagonists have also been used, but there is limited evidence to support their efficacy^{21,32}. Montelukast (Singulair; Merck) and zafirlukast (Accolate; AstraZeneca), are both leukotriene antagonists approved for the treatment of asthma. They reportedly act by inhibiting cysteinyl leukotrienes (leukotrienes C4, D4, and E4) and suppress myofibroblasts³². However, their utility in treating capsular contracture is controversial³².

Prevention of capsular contracture remains the mainstay of treatment with meticulous surgical technique and sterility. Once contracture develops, surgical management remains the only reliable option with surgical excision of part or all of the capsule (capsulectomy) and implant replacement. If contracture recurs, implant removal and failure of reconstruction may occur, a devastating consequence for many women whom breast reconstruction closes the chapter of their oncologic recovery²⁹.

1.5 Radiation-Induced Fibrosis

Ionizing radiation is integral to breast cancer therapy. The therapeutic effect of ionizing radiation is attributed to induction of DNA damage that causes apoptosis of cancer cells³³. Ionizing radiation generates reactive oxygen species (ROS), and these are implicated in the establishment of the late complication of external beam radiation, radiation-induced fibrosis (RIF). RIF can occur in skin and subcutaneous tissue, as well as other organs³⁴. This radiation injury to normal tissue is ultimately the result of persistent inflammation and hyper-activation of fibrotic pathways resulting from both the stimulation of fibroblast proliferation and differentiation into myofibroblasts^{35,36}. Not only is there excessive fibroplasia, but myofibroblasts produce collagen and other extracellular matrix components that culminate in fibrosis and reduce the tissue

compliance³⁴. This reduced tissue compliance impairs the quality of life for cancer patients, and poses challenges to post-mastectomy breast reconstruction. The persistently inflamed micro-environment and myofibroblast survival are considered to be major factors in radiation-induced capsular contracture.

Radiation injury is triggered by a cascade of cytokine activation with TGF- β as the master switch³³. TGF- β signaling is mediated via two cell surface serine/threonine protein kinase receptors³⁷. TGF- β type II receptor first binds TGF- β and presents it to the type I receptor, leading to the formation of a heterotetrameric receptor complex and activation of TGF- β type I receptor. SMAD proteins are a class of proteins that mediate responses to the TGF- β ligands and receptors; activated TGF- β type I receptor induces phosphorylation and nuclear accumulation of SMAD proteins, which then act as transcription factors promoting the expression of various target genes³⁷.

A role for the TGF- β signaling pathway has been reported in one study with respect to development of radiation-induced implant capsular contracture. *Katzel et al* (2011) used SMAD3 knock-out mice to demonstrate the role of TGF- β signaling through phosphorylation of SMAD3 in radiation-induced capsular contracture. They found that irradiated smooth silicone implants, placed dorsally in the knock-out mice, demonstrated few changes on micro-computed tomographic scanning compared to wild-type mice that showed shape and contour deformation³⁸. Histological analysis with hematoxylin and eosin/Alcian blue staining showed differences in capsular thickness with the wild-type mice showing thicker capsules with more disorganization of the collagen fibers. Overall, the results suggested SMAD3/ TGF- β are potential targets for prevention of capsular contracture. The limitations in this study were placement of the implants under dorsal skin of the mice as opposed to ventrally under mammary fat pads, which mimics placement in patients. Multiple sessions of general anesthesia were used to complete the micro-CT scanning, increasing the risk of systemic complications to the mice. Limited histologic analysis of capsular tissue and no immunohistochemistry was performed in this study to establish evidence for fibrosis and capsular contractures. Future studies to further elucidate the TGF- β pathway in radiation-induced capsular contracture are necessary.

1.6 Clinical Grading Scales

1.6.1 Capsular Contracture

The clinical grading of capsular contracture was introduced in 1978 by Baker. This scale is still the most widely used and accepted for clinical classification. It ranges from grade 1 (normal capsule) to grade 4 (severe) (Table. 1)^{39,40}. The Baker grade has been used in animal models of capsular contracture, including porcine and rabbit models, and given that it is a clinical qualitative grading scale it can easily be applied to different species⁴¹⁻⁴⁵.

Table 1. Baker Classification of Capsular Contracture after Augmentation Mammoplasty.

I	Breast absolutely natural; no one could tell breast was augmented	Natural
II	Minimal contracture; I can tell surgery was performed, but patient has no complaint	Palpable
III	Moderate contracture; patient feels some firmness	Visible
IV	Severe contracture; obvious just from observation	Painful

1.6.2 Radiation Injury

The Kumar score is a scale that was originally developed for assessment of radiation injury in the hind leg of mice (Supplemental Figure 1)⁴⁶. Within animal model-based literature, it has been used to provide a high level of detail for cutaneous radiation injury including erythema, dry desquamation, moist desquamation, ulceration, and full thickness injury⁴⁷.

SCORE	SKIN CHANGES
1.0	No effect
1.5	Minimal erythema, mild dry skin
2.0	Moderate erythema, dry skin
2.5	Marked erythema, dry desquamation
3.0	Dry desquamation, minimal dry crusting
3.5	Dry desquamation, dry crusting, superficial minimal scabbing
4.0	Patchy moist desquamation, moderate scabbing
4.5	Confluent moist desquamation, ulcers, large deep scabs
5.0	Open wound, full thickness skin loss
5.5	Necrosis

Supplemental Figure 1. Kumar Scale. A non-linear, semi-quantitative scale to assess radiation skin damage in mice.

1.7 Current Animal Models

There have been numerous published studies using various animal models of capsular contracture. There is great variability in these published models, and there remains a paucity in the literature of a reproducible and robust animal model of radiation-induced capsular contracture. Ideally, there would exist a “gold standard” model that could be used reliably and repeatedly. One variable factor in published studies has been the type of animal used. Rodents remain the most common animal used, with some models using mice, and others that have used rats. There is consensus in the literature that the rat provides a reliable, reproducible and relatively cheap model, while providing accurate histological extrapolation to human tissue⁴⁸. Rats are also larger rodents than mice, which makes any surgical procedure and implant placement easier. In general, the radiation dosages studied in animal models are comparatively higher than human doses, as rodents, and specifically rats, are relatively radio-resistant. For example, Takikawa *et al* developed a rat model of radiation-induced skin ulcers using a single dose of 30 Gy that induced erosion and ulcers at 4 weeks, where they found no visible change with a 10 Gy dose⁴⁹. Optimizing the dose of radiation creates a challenge to any rat model, in

that a high enough dose to induce capsular fibrosis, while minimizing systemic effects and skin ulcers is required.

Wright et al used female Sprague-Dawley rats and placed custom 2mL smooth implants (Mentor, J&J) either subcutaneously dorsal or submuscular below latissimus dorsi⁵⁰. Ten days postoperatively, rats underwent targeted 20 Gy radiotherapy. At 3-months post-operative, both irradiated groups showed hair loss and hyperpigmentation at the radiated site, indicating mild fibrosis. The histologic examination was limited to capsular thickness, that showed no difference between groups. However, the authors comment that the subcutaneous placement showed more morphological and clinical deformation than submuscular placement as viewed on micro-CT.

Diehm et al in their 2019 study used female Lewis rats and miniature textured silicone implants in the submuscular dorsal position⁵¹. At one day post-operative, they delivered a 10 Gy single dose based on *Katzel et al* (2010 and 2011) who found deformational change on micro-CT to a custom implant in mice^{38,52}. *Diehm et al* in their study found capsule thickness was higher in the irradiated group both on MR imaging and histologic analysis. As well, they observed a denser arrangement of collagen fibers accompanied by an overexpression of pro-fibrotic and inflammatory genes CD68 or TGF β -1. They found that injections of collagenase of the bacterium *C. histolyticum* (CCH) reduced capsular thickness, but they experienced hematomas as a complication due to vessel wall thinning from unfractionated irradiation. They then modified their model to deliver the radiation in fractionated doses of 6 fractions of 8 Gy, equivalent to a clinical treatment regimen, as literature suggests increased vessel wall thickness with fractionated dosing⁵³. This radiation delivery was effective at inducing contracture as well, and they did not experience any hematomas with the CCH injections. CCH demonstrated to be effective on reducing capsular thickness and fibrosis.

Eltze et al also used fractionated dosing in their study using male Sprague-Dawley rats and subcutaneous placement of modified textured implant or tissue expander⁵⁴. Radiation was delivered 1-month post-operative using 6-MeV electron beam divided into three fractions of 7.75 Gy each in 5 days for a total dose of 23.25 Gy. They examined fibrosis and capsular contracture qualitatively rating as mild, moderate, and severe and found greater fibrosis in the radiated group at 1-year post-implantation.

Although *Eltze et al* and *Diehm et al* demonstrated induction of capsular contracture with fractionated dosing, which replicates treatment model used in patients, this is impractical in an animal model. This limits the model's reproducibility, given that it requires multiple treatment sessions to coordinate and multiple anesthetics for the animals. *Erpolat et al* (2021) used male Wistar rats, placing a smooth mini silicone implant beneath the panniculus carnosus⁵⁵. Similar to *Wright et al*, they delivered a single fraction of 21.5 Gy external irradiation using a 6-MV linear accelerator. Their aim was to maximize fibrosis and capsular contracture while minimizing the number of anesthetics required. They then evaluated the histologic and immunohistochemical findings at 3 months after radiation. This is in accordance with *Kim et al.* who showed that capsular contracture of irradiated mice had become more apparent at 3 months compared with the findings at 1 month⁵⁶. From these published studies, it is clear that a one-time dose of at least 20 Gy is sufficient to induce minimal contracture, while 30 Gy induces ulcer formation. Therefore, one-time total dosing would be between 20-30 Gy in an ideal model. Although fractionated dosing is effective, it is not efficient for a laboratory model. In terms of follow-up period, 1 month appears sufficient to see an effect, and remains more practical than an extended period of up to 1 year.

These previous rodent models of radiation-induced capsular contracture are not only inconsistent in their radiation dosing, but also their implant type and position. Regarding implant type, various substances have been used as the "implant" ranging from small pieces of silicone sheet to manufacturer supplied custom mini-implants, either with textured or smooth surface. For best reproducibility, a model that uses custom replicate silicone implants by the major implant manufacturers would be ideal, as this would reproduce the implants used in humans. The other limitation is that these previous models have either placed the implants dorsally or mediolaterally in the subcutaneous, sub-panniculus carnosus, or sub-muscular position (sub- latissimus dorsi muscle). To my knowledge, none have yet been reported to place implants sub-mammary, a unique position that replicates placement in patients.

Truong et al has previously developed a novel rodent model of mammary fat pad fibrosis by administering a single dose of gamma radiation (26Gy/11.2min) to the 4th left and right mammary fat pads in retired female Sprague-Dawley breeder rats⁵⁷. Radiation-induced fibrosis was detectable as early as 1-week post-radiation and was substantial by 3-weeks post-radiation.

Molecular and biomarker analyses confirmed that this dose of radiation was sufficient to induce fibrosis of the mammary fat pad. This model provides a basis of radiation-induced mammary fat pad fibrosis that could be easily adapted to include a sub-mammary fat pad implant. Thus, it can be adapted to create a novel rodent model for radiation-induced breast capsular contracture.

2 Thesis Objective and Aims

The main objective of this thesis is to establish a unique *in vivo* rodent model of radiation-induced breast implant capsule contracture that replicates the type of implant and tissue positioning used in humans, that can then be used to identify non-surgical therapies for reducing or preventing capsular contracture.

Objective 1: Modify the previously established rodent model of radiation-induced mammary fat pad fibrosis developed by Truong *et al* to include a sub-mammary gland silicone prosthesis.

Aim 1: Develop a standard surgical procedure in a rodent model that can be easily replicated involving the implantation of a right 4th sub-mammary fat pad silicone prosthesis.

Aim 2: Develop a standard radiation protocol to deliver one-time dose of irradiation to the 4th right mammary fat pad and implant for a total dose of 26 Gy.

Aim 3: After surgery and delivery of radiation treatment; use established clinical assessments of capsular contracture and radiation fibrosis to evaluate for effect.

Objective 2: To assess for radiation-induced fibrosis, of implant capsules and adjacent mammary fat pads, and compare to non-radiated implant capsules and adjacent mammary fat pads.

Aim 1: Use paraffin embedded tissue sections stained for Masson's Trichrome and Picrosirius Red to quantify collagen content and collagen architecture of the right 4th implant capsule and adjacent mammary fat pad in radiated animals compared to non-radiated. As well as in the left 4th mammary fat pad sham surgery tissue samples.

Aim 2: Use tissue hydrolysis assays for hydroxyproline and total protein to quantify the amount of collagen in tissue samples of the right 4th implant capsule and adjacent mammary fat pads in radiated animals compared to non-radiated. As well as in the left 4th mammary fat pad sham surgery tissue samples.

3 Methods

All experiments were approved and compliant with the standard operating protocols of the Animal Use Subcommittee (Protocol # 2017-153) at Western University in London, Ontario, Canada.

All animal work was conducted at London Health Sciences Centre, London Regional Cancer Program (LRCP), and Health Sciences Animal Research Facility, Western University.

3.1 Animal Experiments Overview

Experiments were conducted using Sprague Dawley retired female breeder rats (Charles River) to determine the dose of radiation required to induce clinically detectable fibrosis and implant capsular contracture. Rats were caged in pairs, in a temperature-controlled room, with a 12-hour light/dark cycle, and were provided water and a standard rat diet. One rat was kept as a control (no surgery, no radiation). Figure 1 outlines the experimental overview. Thirteen rats underwent implant surgery (described below), with seven rats then receiving radiation to the implant 4-5 weeks post-operatively (surgery, radiation). Six rats were kept as non-radiated implant surgery controls (surgery, no radiation). Experiments were done in two sets. The first set having five animals total - 3 surgery/radiation, 1 surgery/non-radiation, and the single control animal. The surgery protocol and radiation delivery was determined to be technically feasible in the first set of animals and thus, the second set was then completed with four additional surgery/radiation rats (7 total) and five surgery/non-radiation rats (6 total).

Power analysis and sample size calculation was performed using the following equation for a qualitative endpoint between two groups⁵⁸: $\text{Sample size} = 2 (Z_{\alpha/2} + Z\beta)^2 \times P(1 - P)/(p_1 - p_2)^2$. A power of 0.8 and significance level of $p < 0.05$ was used. The endpoint used was the development of clinically detectable capsular contracture. The prevalence in the case (radiated) group (p_1) was assumed to be 100% or 1.0, and the prevalence in the control (non-radiated) group (p_2) 20% or 0.2 based on the rate in the literature of development of capsular contracture without radiation.

$Z_{\alpha/2} = Z_{0.05/2} = Z_{0.025} = 1.96$ (From Z table) at type 1 error of 5%

$Z\beta = Z_{0.20} = 0.842$ (From Z table) at 80% power

$P = \text{Pooled prevalence} = (\text{prevalence in case group } [p1] + \text{prevalence in the control group } [p2])/2$
 $= (1 + 0.2) / 2 = 0.6$

$\text{Sample size} = 2 (Z_{\alpha/2} + Z_{\beta})^2 \times P (1 - P) / (p1 - p2)^2 = 2(1.96 + 0.842)^2 \times 0.6 (1-0.6) / (1-0.2)^2 = 5.88$.

Thus, a sample size of 6 rats was calculated per group, and accounting for a 10% attrition rate, 7 rats per group would be needed. Unfortunately, one rat in the non-radiation group died unexpectedly after receiving the animals at our facility. This was prior to the beginning of the experiments, and was not an adverse event of the protocol. The timing between the two sets of animal experiments was unintentionally extended due to the COVID-19 pandemic.

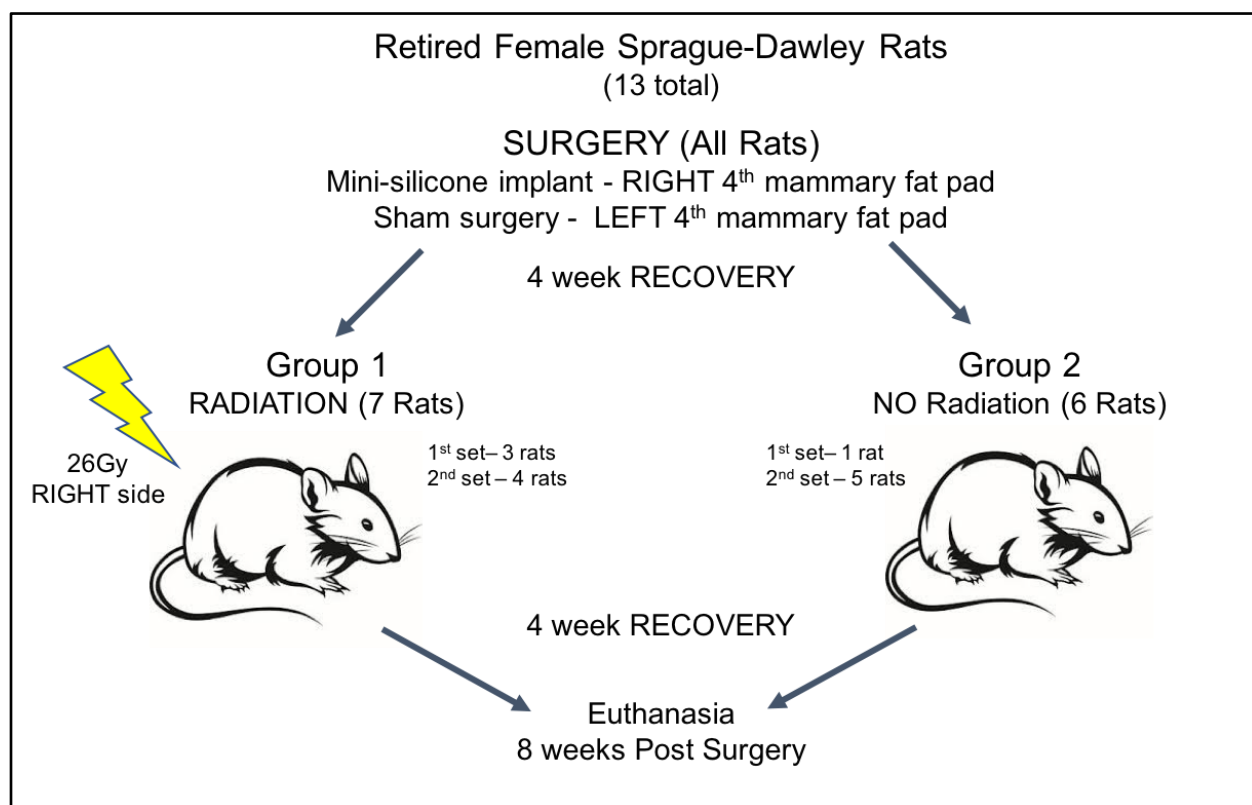


Figure 1. Animal Experiment Overview.

3.2 Surgery

Surgery was conducted at the LRCP animal facilities. Animals were weighed then administered a single dose of Meloxicam (1-2mg/kg) thirty minutes pre-operatively. Animals were then induced and maintained with isoflurane gas anesthesia via a nose cone for the surgery (Figure 2). Rats were positioned supine on a warming pad and limbs secured in position with tape. Lubricant was used to protect the eyes. Temperature was then measured. Hair over the 4th set of mammary fat pads was then clipped in a 2cm diameter centered around the nipple. Skin was prepped with antiseptic scrub (chlorhexidine) followed by alcohol wipe and then final application of antiseptic solution (betadine). On the right and left side, an incision was made through the skin and subcutaneous tissue below the 4th mammary fat pad, a pocket was then dissected below the fat pad with scissors (Figure 3). On the right side, a 2cc custom “mini” cohesive silicone gel implant (Mentor, Johnson&Johnson) was placed in the pocket after being irrigated with betadine. Dimensions of the implant are 2cm diameter and 1cm projection (height) (Figure 4). On the left side, no implant was placed (sham surgery). The incisions on both sides were then closed with an absorbable suture and secured with skin glue. Animals were then administered oxygen vis nose cone until awoken from anesthesia and then transferred to a clean bed for recovery.



Figure 2. Rat surgery set-up. Gas anesthesia provided via nose cone with 4th set of mammary fat pads clipped in preparation.

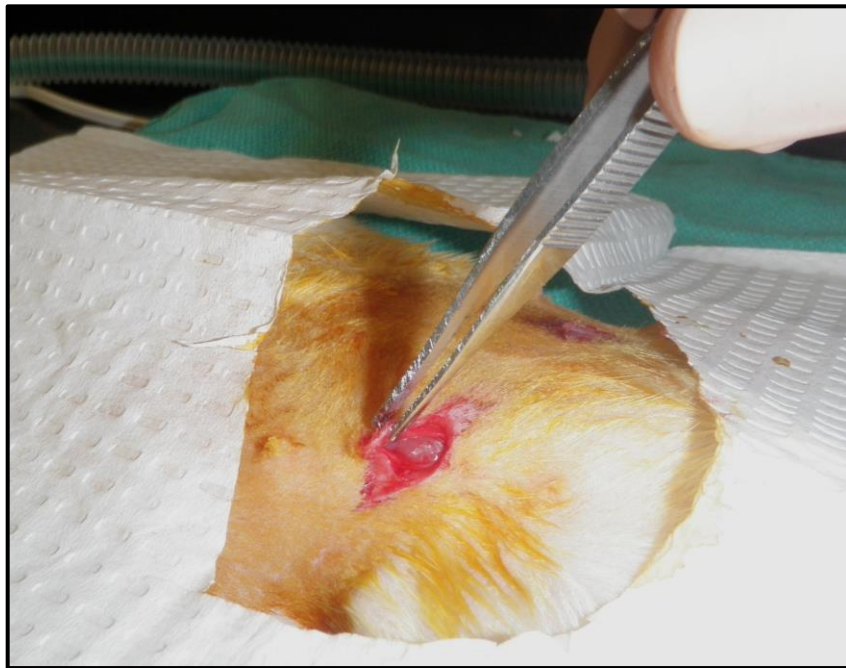


Figure 3. Intraoperative image of rat implant surgery demonstrating the pocket created below the right 4th mammary fat pad.

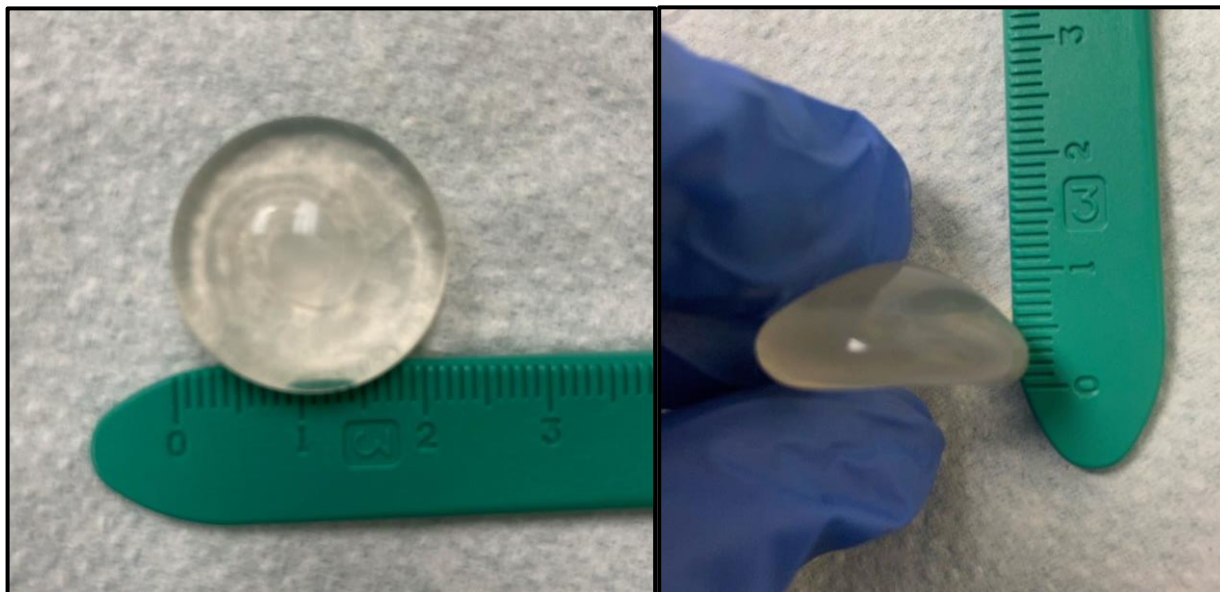


Figure 4. “Mini” cohesive silicone gel implants supplied by Mentor/J&J. Base diameter is 2cm, and projection of the implants is 1cm.

3.3 Post-Operative Monitoring

Animals were monitored daily for the first 7 days post-operatively and then weekly thereafter. Meloxicam was administered (1-2mg/Kg) on post-operative day 1. Weight was recorded along with recording behaviour, appearance, activity, and examining the surgical site for complications. The rats that did not undergo radiation treatment were continued to be housed and monitored at LRCP until 8 weeks post-operative. The implant was examined weekly for evidence of capsular contracture and given a Baker grading score.

3.4 Irradiation

The animals in the radiation group underwent irradiation to the implant at 4-5 weeks post-operatively. The initial set with three rats underwent radiation at 5 weeks, and the second set of four rats at 4 weeks. The difference in radiation timing between the groups was due to scheduling constraints. The irradiation was carried out at the LRCP using a clinical linear accelerator (Clinac 21iX, Varian Medical Systems, Palo Alto, CA) for a total of 26Gy (2600MU

at 600MU/min). A total dose of 26Gy was chosen as this dose was able to induce clinically detectable fibrosis of the mammary fat pad by 1 week in the paper by *Truong et al.* As well, based on previous animal studies, as described in Chapter 1.7, it is clear that a one-time dose of at least 20 Gy is sufficient to induce minimal contracture, while 30 Gy induces ulcer formation. The lowest energy photon beams at 6MV was employed and a target field of approximately 3 cm x 3 cm was used with the mammary fat pad and implant centered in the beam. This is in contrast to *Truong et al* where a field size of 1cm was used with a lower energy beam (100 kV). With the addition of sub-mammary fat pad silicone implants, a larger field with 0.5 cm margin was needed to cover the size of the implant (2cm diameter). Max dose was at a depth of 1-1.5cm in water, and the acrylic plastic animal holding box provided the buildup to the maximum dose.

Animals were induced and maintained with isoflurane gas anesthesia via nose cone for the irradiation. For the initial set of three animals, the rats were positioned within the induction chamber on their sides on a foam pad in lateral decubitus position, with the implant on the right isolated away from the abdomen using plastic positioning sticks (Figure 5). Gantry angle of the photon beam was such that the beam was pointed directly down onto the implant on the animal's right side.

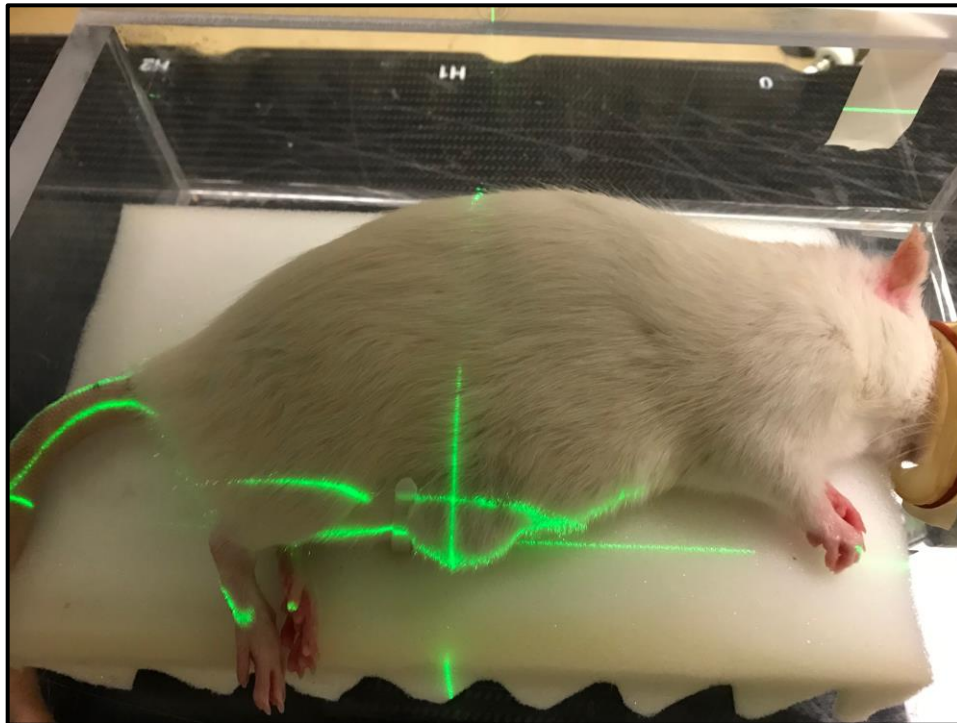


Figure 5. First set of rats receiving radiation treatment were positioned in the induction chamber in the lateral decubitus position on a foam pad. The implant and fat pad isolated from the body using positioning sticks.

After the initial set of animals, a 3D printed platform (“ratform”) was created for the animals to be positioned upon. The platform allowed the animals to be positioned prone in the induction chamber, with an open trough running the length of the platform the width of the implant (Figure 6). This allowed the implant to fall below the level of the platform and for the remainder of abdominal tissue to be blocked (Figure 7). This allowed for consistent isolation of the implant and overlying fat pad, while limiting radiation to surrounding tissue and abdominal organs. A lateral opposed pair of 6MV photon beams (at 90° and 270° gantry angles) was employed for the irradiation. Using the room lasers, the implant was first centred at the isocentre of the linear accelerator. We then dropped the couch until the vertical position of the isocentre lined up at the level of the platform so that we can employ asymmetric jaws to avoid irradiating the rest of the rat due to beam divergence. For example, for the 90° beam, we used the following jaw settings (at 0° collimator rotation): X1 = 0 cm, X2 = 3 cm, Y1 = 1.5 cm, Y2 = 1.5 cm, resulting in a 3 cm x 3 cm field size that encompasses the implant with a margin.

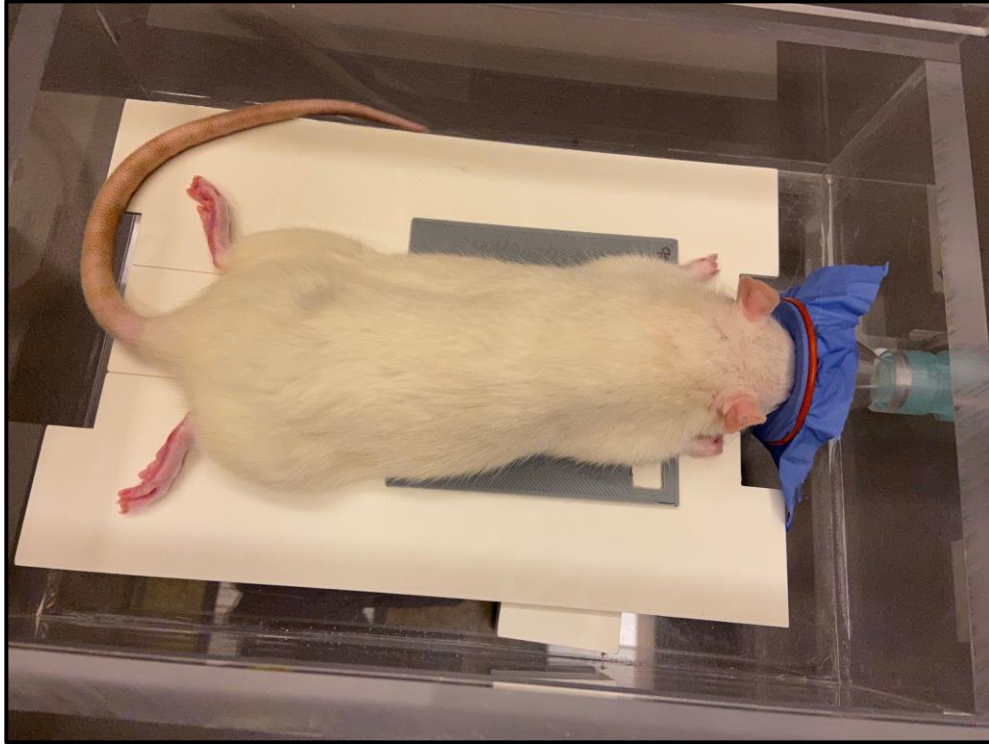


Figure 6. The second set of rats receiving radiation treatment were positioned using a 3D printed platform “ratform” in the prone position within the induction chamber.

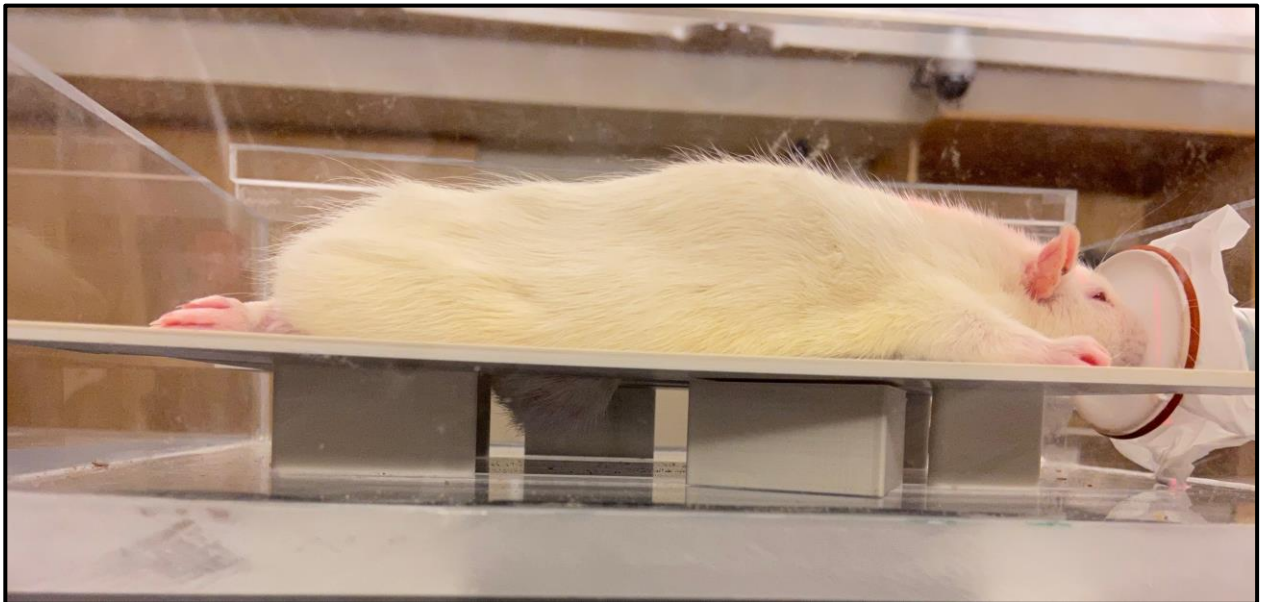


Figure 7. Side view demonstrating the implant and overlying fat pad falling through the platform to isolate away from the remainder of the body. The supporting blocks are movable to allow alignment of the implant with the lasers. A pair of lateral parallel opposed beams were used to irradiate the implant, sparing the rest of the rat. A 3D printed block (designed to have 1.0 cm water equivalent) was then placed next to the implant to act as build up for the beam.

3.5 Post-radiation Monitoring

Once the treatment was complete, the animals were then administered oxygen vis nose cone until awoken from anesthesia and transferred to a clean bed for recovery supplied with fresh water. Animals were then housed at the Health Sciences Animal Research Facility, Western University, for 4 weeks following radiation and provided with water and standard rat diet. According to a study by Sengupta et al., 1 month of an adult rat's life equates to 3 human years⁵⁹.

The animals were housed at Western University and monitored daily for 7-days post-radiation, and then twice weekly. Weight was recorded along with recording behaviour, appearance, activity, and examining the radiation site for complications. The Kumar scale was used to grade radiation changes at 7-days and 4-weeks post-radiation (prior to euthanasia). The Kumar scale was chosen as it was designed to detect radiation skin damage in rodent models. *Truong et al* found, that clinically detectable differences were found in radiated versus non-radiated rodents using the scale. The implant was examined weekly for evidence of capsular contracture and given a Baker grading score. The Baker grading score is the standard for clinically rating capsular contracture, and has been used in animal models previously. As palpation is required to give a grade, the assessment could not be blinded.

3.6 Euthanasia and Tissue Harvest

Animals were euthanized at 8-weeks post-surgery (4-weeks post-radiation). Non-radiated animals were euthanized at LRCP and radiated animals at Western Health Sciences Animal Research Facility. Animals were euthanized in a Carbon Dioxide (CO²) chamber according to the AUP. Second method of confirmation of death was used by laceration of femoral artery after tissue harvest.

Animals were secured using tape to dissection surface (surgical towel on board). Photos were taken for each animal. A 15-blade was used to make a longitudinal midline incision from the xiphoid process down to the pubis, and transversely to the mid-axillary line at these landmarks. Dissection was then carried along an alveolar plane, deep to the level of the mammary fat pad (left side) or deep to implant capsule (right side) and superficial to the parietal peritoneum. The

fourth mammary fat pad was identified by deep yellow adipose tissue. For consistency, the area of dissection included the subcutaneous tissue up to the level of the xiphoid process for the cephalad border, the dorsal border of the fat pad, the most ventral-medial border of the fat pad, and to where a blood vessel to the fourth mammary fat pad emerges as the caudal border of the fat pad. Dissection of the subcutaneous tissue including the mammary fat pad was carried down to the plane between dermis and subcutaneous fat. On the right side, the fat pad, implant, and capsule were dissected en bloc (Figure 8). On the left sham surgery side, the fat pad alone was dissected (Figure 9). An additional fat pad in the 5th nipple set was taken as an intra-rat control in each rat in the first set of animals.

Tissue from two animals (second set experiments) from both the non-radiated group and the radiated group for both left sham and right implant were divided in half (implant removed) and one half stored in -80 degrees Celsius for use in Western Blots while the other half was fixed in 10% neutral buffered formalin for 48 hours for tissue sectioning. The remaining tissue samples from the other animals were left intact and fixed in 10% neutral buffered formalin for 48 hours prior to tissue sectioning.

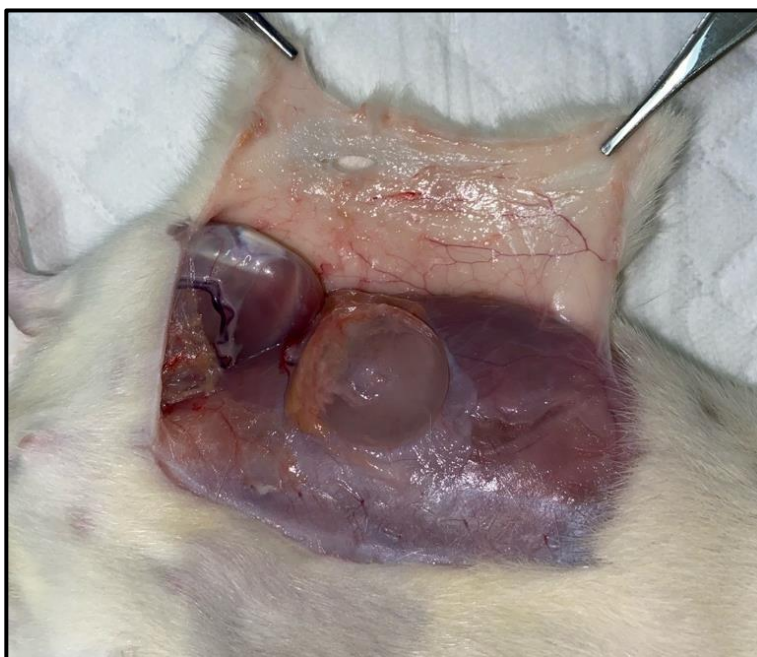


Figure 8. Demonstration of tissue harvest on right 4th mammary fat pad with implant and capsule en bloc. Dissection included fat pad from xiphoid cranially, extent of pad dorsal and ventral, and the caudal extent being the blood vessel to the 4th fat pad.

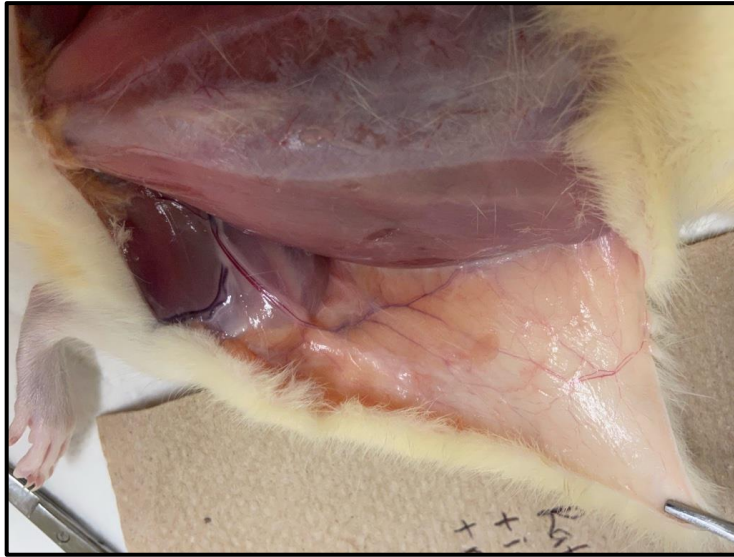


Figure 9. Demonstration of left 4th mammary fat pad tissue harvest. The fat pad is demonstrated not yet harvested. The tissue harvest includes the yellow fat from xiphoid cranially to the blood vessel to 4th pad caudally, midline ventrally, and the dorsal extent of the fat pad.

3.7 Tissue Sectioning

The fixed tissue was then processed for paraffin embedding. The tissue was oriented and embedded in paraffin wax. The samples with the implant in situ were embedded with the implant to maintain capsular architecture. Once embedded, the implant containing samples were then sliced down to the capsule, the implant was removed and the remaining space was filled with paraffin wax for sectioning. Slides for H&E and Masson's Trichrome were sectioned at 5 μ m, and slides for immunohistochemistry were sectioned at 4 μ m. Sections for H&E were taken on plain glass slides, and sections for Masson's Trichrome and immunohistochemistry were taken on Superfrost Plus "charged" slides, for extra adhesion. Microm HM200 Ergostar (GMI; Ramsey, Minnesota, USA) and Leica RM 206 microtomes were used for sectioning.

3.8 Tissue Histology

3.8.1 Hematoxylin and Eosin

Tissue sections were stained with Hematoxylin and Eosin (H&E). Sections from all animals in the study were included. Two slides per animal were stained, one from the right mammary fat pad and implant capsule, and one from the left sham surgery mammary fat pad. H&E slides were

imaged using the Aperio ImageScope, (Leica Microsystems, Buffalo Grove, IL, USA) and the software was used for image acquisition. Images of the entire slide, as well as six randomized images at 10X magnification were taken of areas that contained capsular tissue (right side), or fat pad alone (left side).

3.8.2 Masson's Trichrome

Tissue sections were stained for collagen using Masson's Trichrome (Cat # SLBN7822V, Sigma-Aldrich, Darmstadt, Germany). Sections from all animals in the study were included and two slides per animal were stained, one from the right mammary fat pad and implant capsule, and one from the left sham surgery mammary fat pad. Masson's Trichrome slides were imaged using the Aperio ImageScope (Leica Microsystems, Buffalo Grove, IL, USA) and the software was used for image acquisition. Images of the entire slide, as well as six randomized images at 10X magnification were taken of areas that contained capsular tissue and adjacent fat pad (right side), or fat pad alone (left side). Masson's trichrome highlights collagen fibers, with collagen staining blue. Increased blue staining indicates greater collagen content in the tissue sample.

Image analysis was carried out using ImageJ software (U.S. National Institute of Health, Bethesda, Maryland, USA). Images were de-convoluted using the pre-programmed function for Masson's Trichrome and the image selecting for blue pixels was used. The polygon function was used to select for the area containing capsular tissue. The size of the area containing capsular tissue and the mean grey value of this area was measured. The mean grey value for 6 regions of interest (ROIs) for each animal were averaged, with higher grey values corresponding to more stain uptake, and thus higher collagen content. The mean grey value for the radiated animals was compared to the non-radiated animals using the Mann Whitney U-test for significance.

3.8.3 Picrosirius Red

Tissue sections were stained for collagen using Picrosirius Red Staining Kit (Cat # 2490-250, Polysciences, Warrington, PA) with the help of the Molecular Pathology Lab at Robarts Research Institute. Five sections per animal were stained, including all right mammary fat pad and implant capsule samples (6 non-radiated, 7 radiated), and five left sham surgery fat pad samples (2 non-radiated, 3 radiated). Slides were examined under polarized light and six ROIs at 40X magnification were taken of each slide, focusing on capsular and adjacent mammary fat pad

tissue (right side), or mammary fat pad (left side). Abrio 2.2 (Cri, Woburn, MA, USA) software was used for image acquisition. Images were captured by a blinded assessor and saved in Grayscale and Pseudocolor format.

Analysis was carried out using ImageJ software (U.S. National Institute of Health, Bethesda, Maryland, USA). Under polarized light, there is differing birefringence colours that are dependent on collagen fiber thickness and alignment. Increasing fiber thickness is observed through changes in colour from blue to yellow to orange to red. Thus, expression of red, or denser collagen bundling in the tissue is typical of fibrosis. Conversely, blue reflects a lower density of collagen bundling. The threshold function in ImageJ was used to measure the amount of red, orange, yellow, and blue in the six ROIs containing capsular tissue for each animal (5 slides per animal). Each 40X image was reviewed and all images containing capsular tissue were selected for analysis. The images were then cropped for the area containing capsule, in order to eliminate the adjacent fat pad. For the left 4th sham surgery tissue sections the whole 40X image was used for pixel quantification. The number of pixels for each image were then measured using the following hue definitions: red 2-9 and 230-256, orange 10-38, yellow 39-51, blue 52-128⁶⁰. The difference in red and blue pixels for right 4th implant capsule in radiated animals were compared to non-radiated animals using Mann Whitney U-test. Like-wise the left 4th sham fat pads in radiated and non-radiated animals were compared. In order to account for varying amounts of tissue in the images, we also expressed the red and blue pixel count as a proportion of total pixels (i.e. ratio of red to blue pixels).

3.9 Tissue Assays - Hydroxyproline to Total Protein Assay

The second method of quantifying fibrosis in the tissue samples was through tissue hydrolysis assays for hydroxyproline (Cat #K555-100, Biovision, Milpitas, Ca, USA) and total protein (Cat #QZBtotprot1, Quickzyme Biosciences, Leiden, Netherlands). The amount of hydroxyproline in a tissue sample was used as a measurement of collagen, and standardized against the amount of total protein in the sample to account for any difference in the amount of tissue in each of the hydrolysates. A higher ratio would indicate higher collagen content and thus, more fibrosis. Tissue samples were prepared and hydrolyzed according to the assay's instruction manuals. Twenty-five 10uM sections from the right 4th implant capsule and mammary fat pad from each animal in both groups were used (6 non-radiated, 7 radiated). Six technical replicates were run

per sample. Twenty-five 10uM sections from the left 4th mammary fat pad sham surgery from two animals in both groups were used (2 non-radiated, 2 radiated). Six technical replicates were run per sample.

Standards were prepared according to manufactures instructions. The standards and experimental sample assays were run in 96-well plates, and absorption was read at 570nm and 560nm for total protein and hydroxyproline respectively using Biotek plate reader Synergy HTX (Biotek Instruments, Winooski, Vt, USA). The standard curve was then used to calculate the amount of hydroxyproline (ug) and total protein (ug) per well. For each technical replicate, a ratio of hydroxyproline to total protein was calculated. Scatter plots were used to detect outliers, that were then excluded from analysis. The average of the technical replicates was then calculated to get an overall ratio for each sample. The samples in the non-radiated group and the radiated group were then averaged and compared using the Mann Whitney U-test to detect significant differences in collagen to total protein ratio.

4 Results

4.1 Clinical Assessments

All non-radiated animals developed Baker grade 1 capsules that remained soft and mobile throughout the 8-weeks post-operative period. All animals were given a Kumar scale score of 1 or no effect (Figure 10). One animal did develop a post-operative infection on the implant side that required BNP ointment and isolation of the animal. This went on to heal with no consequence, and the implant remained soft and mobile with a Baker grade 1 capsule.

A total of seven animals received post-operative radiation treatment. The initial set of three animals received 26Gy total dose of radiation to the 4th right mammary fat pad and implant. Prior to radiation, all three animals demonstrated implants that had a Baker grade 1 capsule, being soft and highly mobile. At post-radiation day 7, the Kumar scale score for all animals was 2, demonstrating erythema and dry desquamation. By 4-weeks post-radiation, there was hair re-growth at both the 4th right and left mammary fat pads and the skin had returned to normal (Kumar scale 1). All three animals demonstrated implants that felt firm and less mobile post-radiation, and were graded as Baker grade 2 contractures (Figure 11).

After this initial set of experiments demonstrating technical feasibility of the implant surgery, as well as radiation delivery, improvements in animal positioning and radiation dose delivery were made with the 3D printed “ratform”. The second set of four animals also received a total of 26Gy to the 4th right mammary fat pad and implant. Prior to radiation, again all animals had a Baker grade 1 capsule. At post-radiation day 7 the animals demonstrated Kumar scale score of 2-2.5 demonstrating erythema and desquamation. By post-radiation week 4 the animals started to develop minor dry scabbing and maintained hair loss (Kumar scale of 3-3.5). All implants developed contracture of Baker grade 3, feeling firm, immobile, and becoming visible. There were noted changes to the 4th left mammary fat pad area (sham surgery), with loss of hair and mild erythema (Figure 12). There were no systemic complications or adverse effects in any of the radiated animals.

Results from the second set of radiation showed that the delivery was improved with use of the 3D printed “ratform”. This is demonstrated by the second set of animals showing more acute

skin changes such as mild scabbing and persistent hair loss at 4-weeks post-radiation. Both set one and two of radiated animals showed clinical evidence of capsular contracture with at least Baker grade 2, or palpable firmness, with the second set becoming more visibly contracted, or a Baker grade of 3.

Table 2. Kumar score and Baker grade for animals undergoing Surgery with Silicone Implant and Post-Operative Radiation to Right 4th Mammary Fat Pad.

Animal Subject Number	Radiation	Baker Grade Pre-Radiation	Kumar Score Post-Radiation Day 7	Baker Grade Post-Radiation Week 4	Kumar Score Post-Radiation Week 4
1-1	Y	1	2	2	1
1-3	Y	1	2	2	1
1-4	Y	1	2	2	1
2-1	Y	1	2.5	3	3
2-2	Y	1	2.5	3	3.5
2-3	Y	1	2	3	3.5
2-4	Y	1	2	3	3

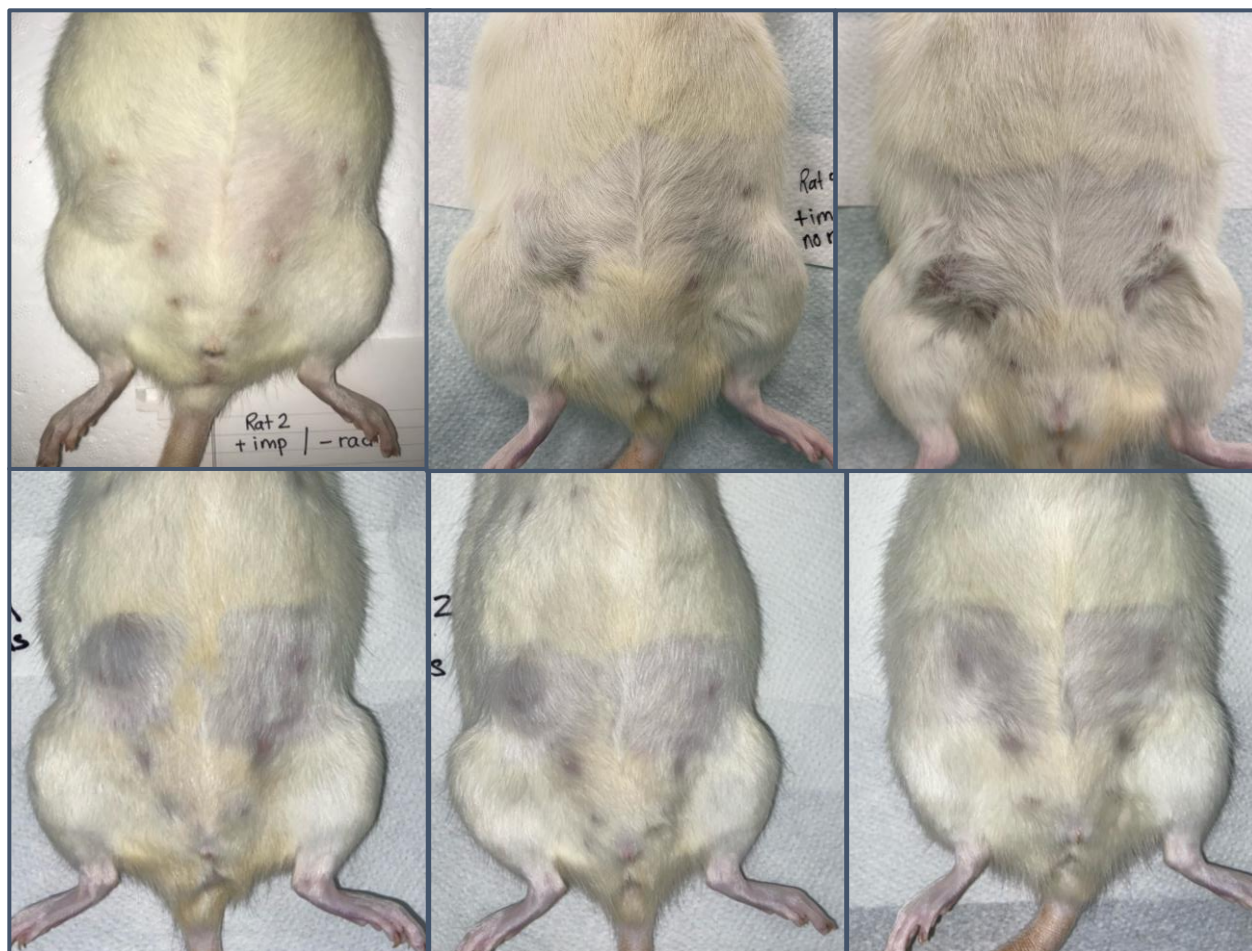


Figure 10. Photographs of non-radiated rats at 8-weeks post-surgery with 4th right implant sub-mammary fat pad. Left 4th mammary fat pad sham surgery. All rats demonstrate a Baker Grade 1 capsule.

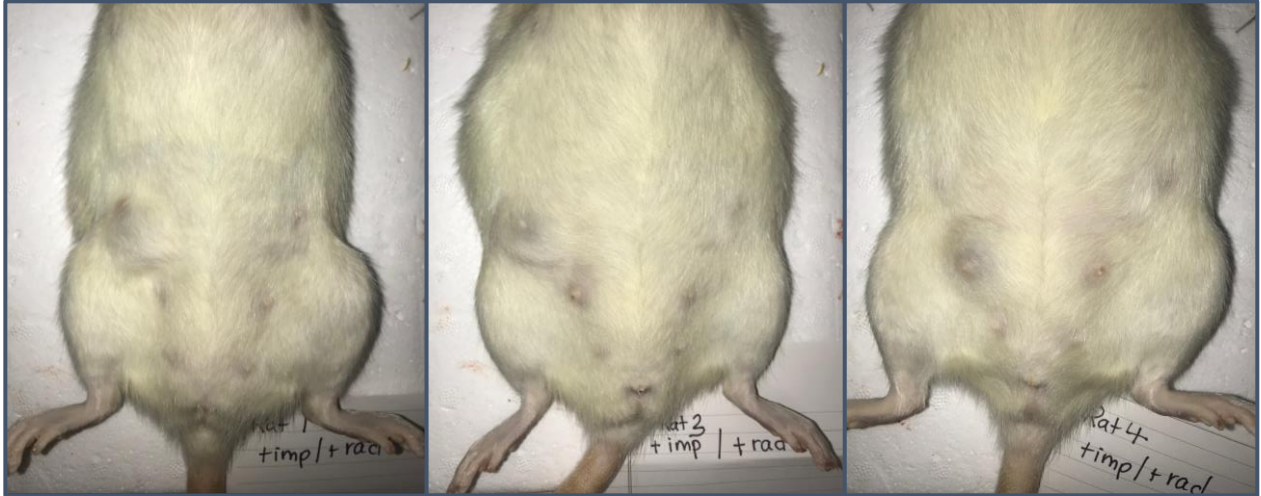


Figure 11. Photographs of first set of rats at 4-weeks post-radiation treatment to the 4th right implant and mammary fat pad. Left 4th mammary fat pad sham surgery. All three animals demonstrate Baker Grade 2 firm capsules.

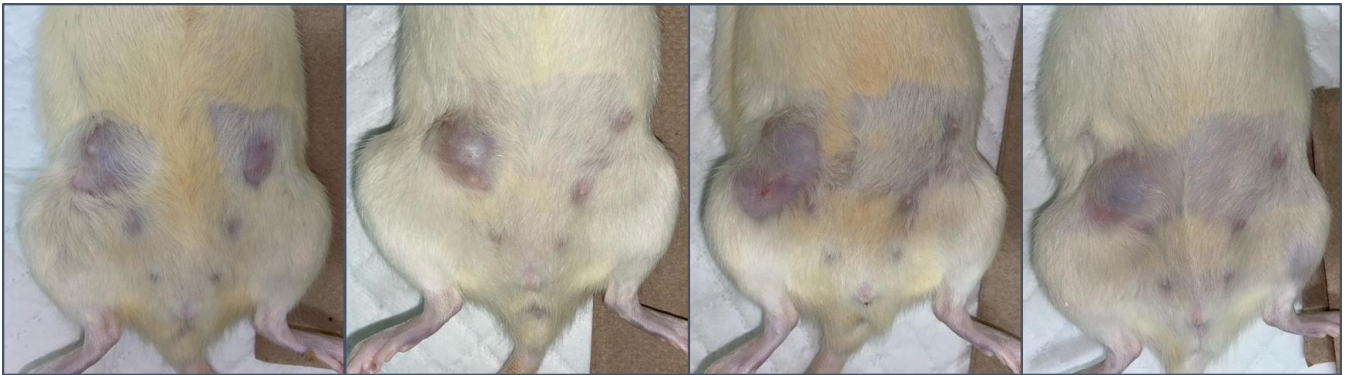


Figure 12. Photographs of second set of rats at 4-weeks post-radiation treatment to the 4th right implant and mammary fat pad using the 3D printed "ratform". Left 4th mammary fat pad sham surgery. All animals demonstrate Baker Grade 3 capsules, and show persistent hair loss.

4.2 Masson's Trichrome

Qualitatively greater blue staining, and therefore greater collagen content, was observed with Masson's trichrome for the tissue sections from radiated implant capsules compared to non-radiated capsular tissue (Figure 13 and 14). Quantification of blue pixel density using ImageJ software revealed overall mean higher density in the 4th right implant capsular tissue radiated group compared to non-radiated group (120.08 vs 94.56, $p < 0.05$) (Figure 15). This indicates that in radiated implants, there is greater collagen in the capsule. For the tissue sections taken from the left 4th fat pad sham surgery, there was no significant difference between the radiated and non-radiated animals (35.32 vs 31.54, $p = 0.47$) indicating that the radiation did not induce fibrosis on the left sham surgery side (Figure 14). Both the radiated and non-radiated right 4th implant capsular tissue groups had significantly higher blue pixel density when compared to the left 4th sham surgery radiated and non-radiated groups ($p < 0.05$) indicating that with the formation of an implant capsule there is greater collagen in the tissue sections.

When comparing the tissue samples from the first set of radiated animals to the second set of animals ("ratform") no significant difference was found in blue pixel density (117.48 vs 122.03, $p = 0.38$). The density of blue pixels was significantly higher for both radiated groups when compared to the non-radiated group (117.48 vs 94.56, $p = 0.03$; 122.03 vs 94.56, $p = 0.008$) indicating that both methods of radiation set-up (displacement vs "ratform") induced fibrosis as measured by increased collagen content (Figure 16).

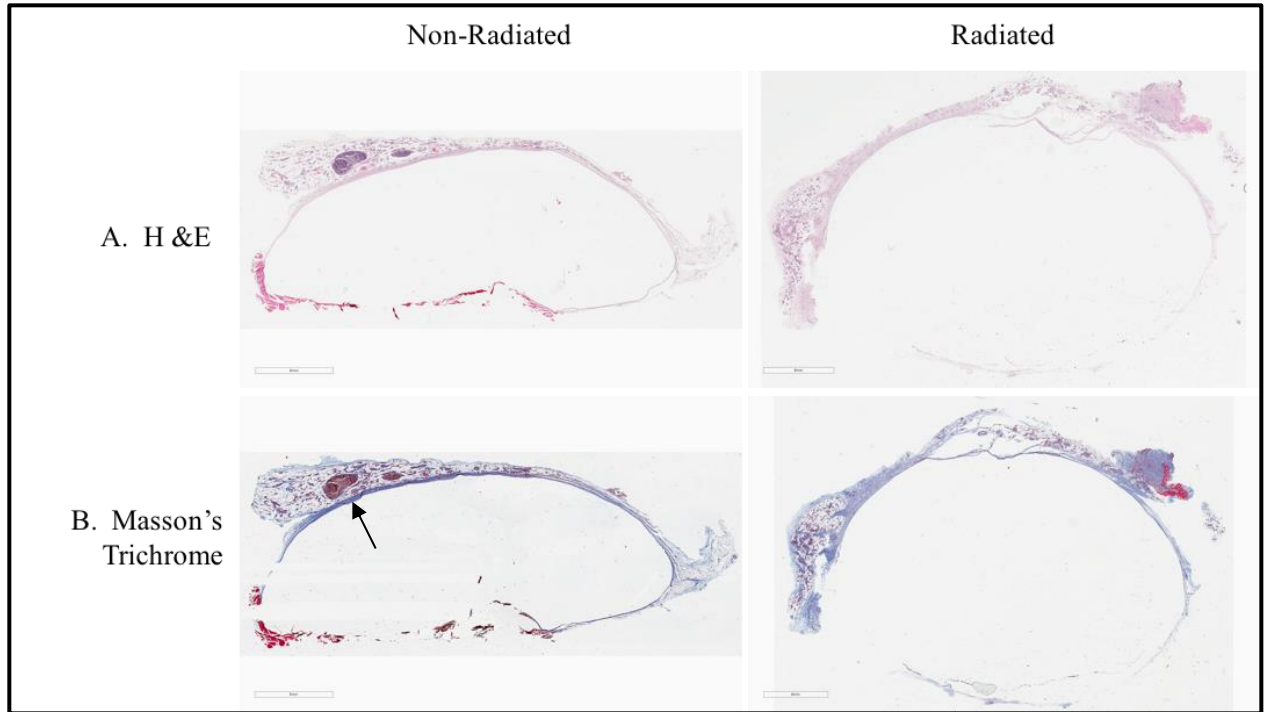


Figure 13. Representative images of paraffin embedded tissue sections from non-radiated and radiated animals containing right 4th implant capsule and adjacent fat pad with architecture of the capsule preserved. Arrow points to capsule. A. H&E B. Masson's Trichrome.

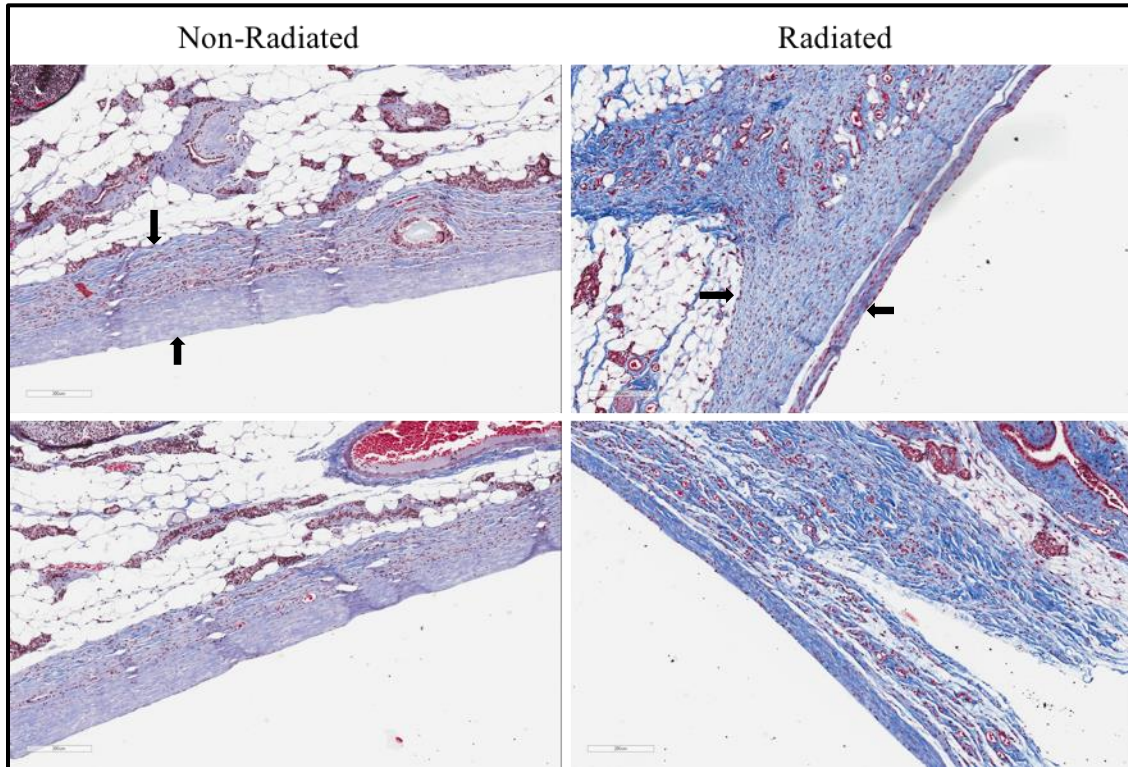


Figure 14. Paraffin embedded tissue sections from non-radiated and radiated right 4th implant capsule and adjacent fat pad were stained with Masson's Trichrome. Arrows denote capsule layer. Darker staining indicates greater collagen concentration. Two representative images each from one non-radiated and one radiated animal at 10X.

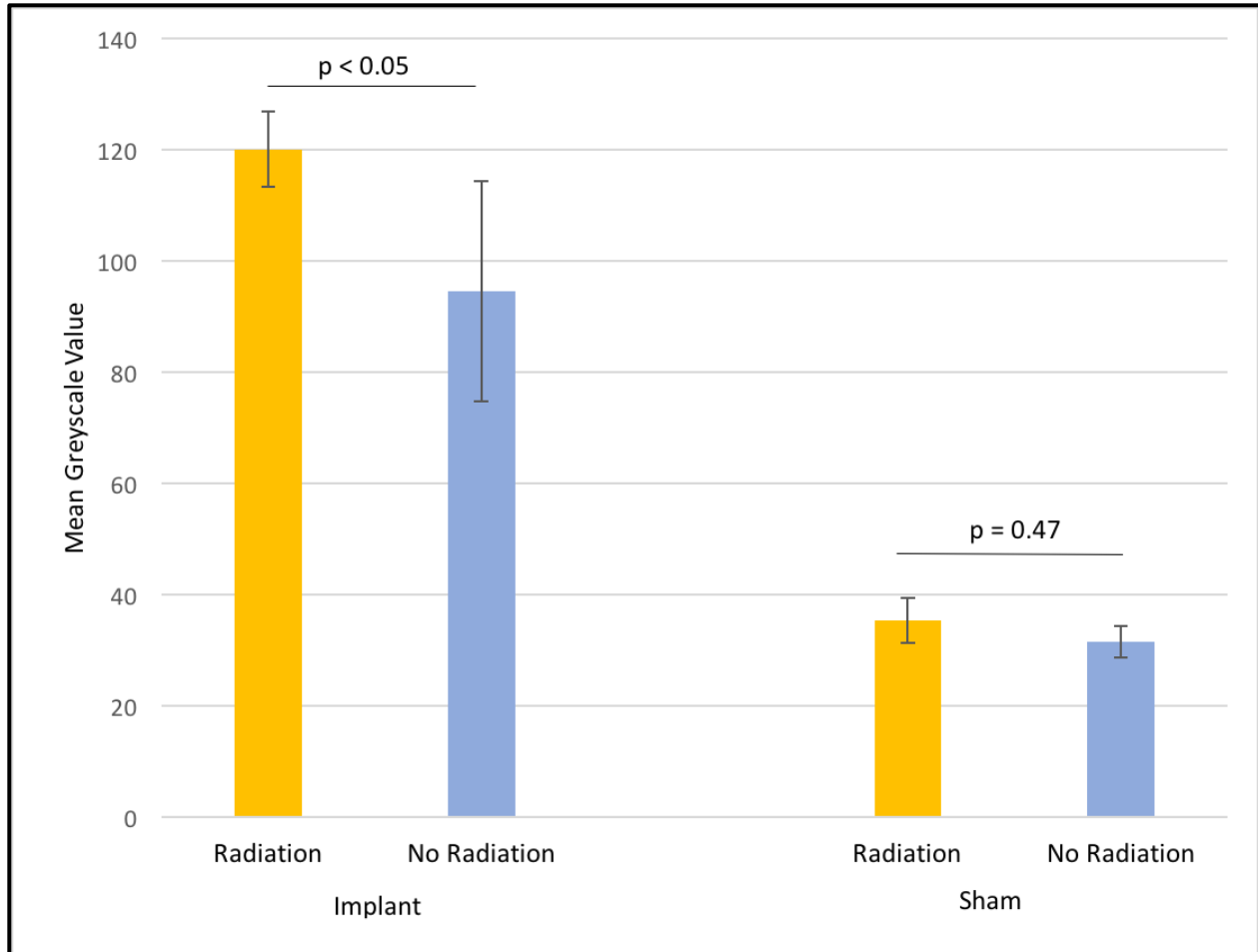


Figure 15. Masson's Trichrome image analysis using ImageJ software quantifying the mean greyscale (blue pixel density) in the right 4th implant capsule tissue and fat pad and left 4th sham surgery fat pad from radiated ($n=7$) and non-radiated animals ($n=6$), 6 ROIs per animal.

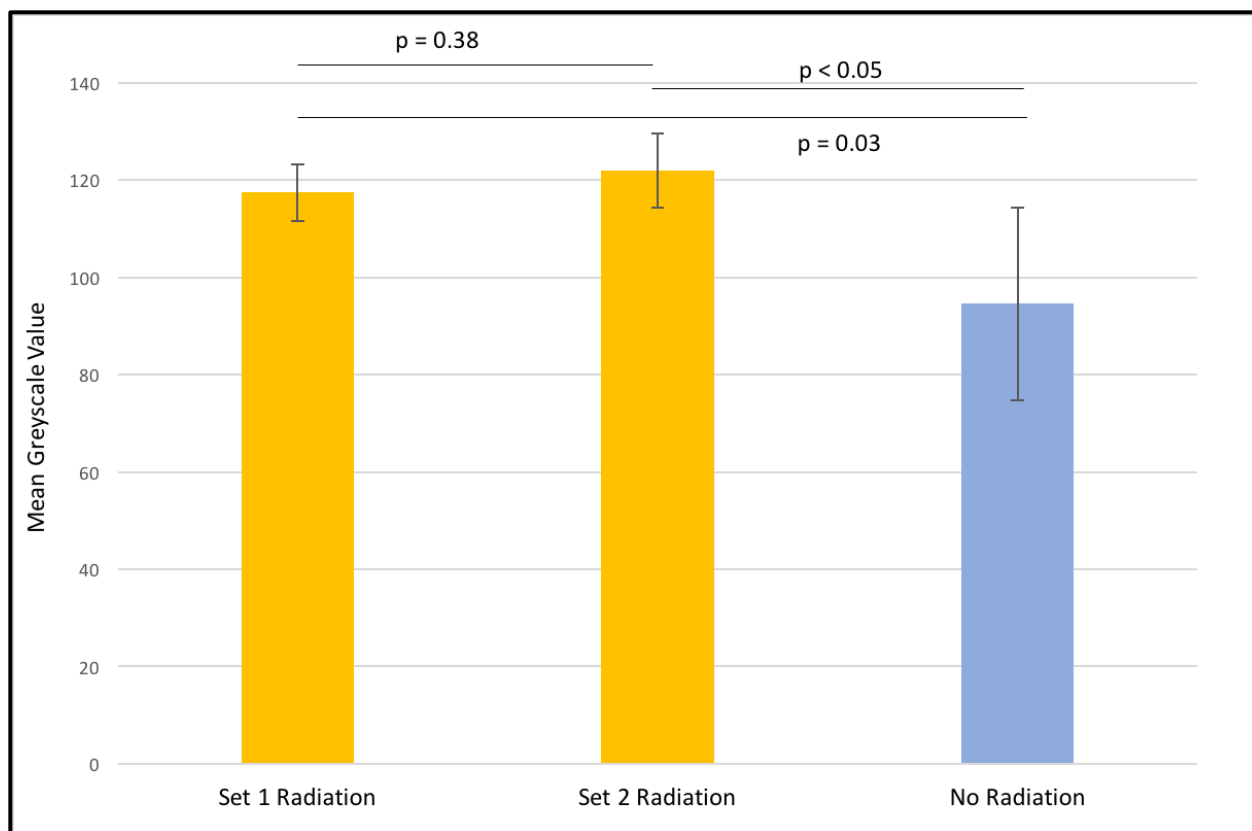


Figure 16. Masson's Trichrome image analysis using ImageJ software quantifying the mean greyscale (blue pixel density) in the right 4th implant capsule tissue and fat pad from Set 1 radiated animals ($n=3$), Set 2 radiated animals ("ratform", $n=4$), and non-radiated animals ($n=6$). 6 ROIs per animal.

4.3 Picrosirius Red

Reviewing the 40X images for picrosirius red staining showed variability in the area of the tissue section captured. The images were captured by a blinded assessor, and although instructed to capture ROIs that contained capsule, there were some images that did not contain any capsular tissue, and thus, these were excluded from analysis. For one animal from the radiated right 4th implant group, none of the captured images of the tissue sections contained capsule tissue. This animal was excluded from analysis.

Picrosirius red staining under polarized light shows fibril formation, with increasing fiber thickness when going from blue to red, with red indicating denser collagen bundling. On qualitative review of the images that contained capsule, the radiated tissue sections appeared to have more red staining than non-radiated within the implant capsule. Figure 17 and 18 show

representative images for tissue sections of right 4th implant capsule and adjacent fat pad in radiated and non-radiated animals at 10X and 40X, respectively.

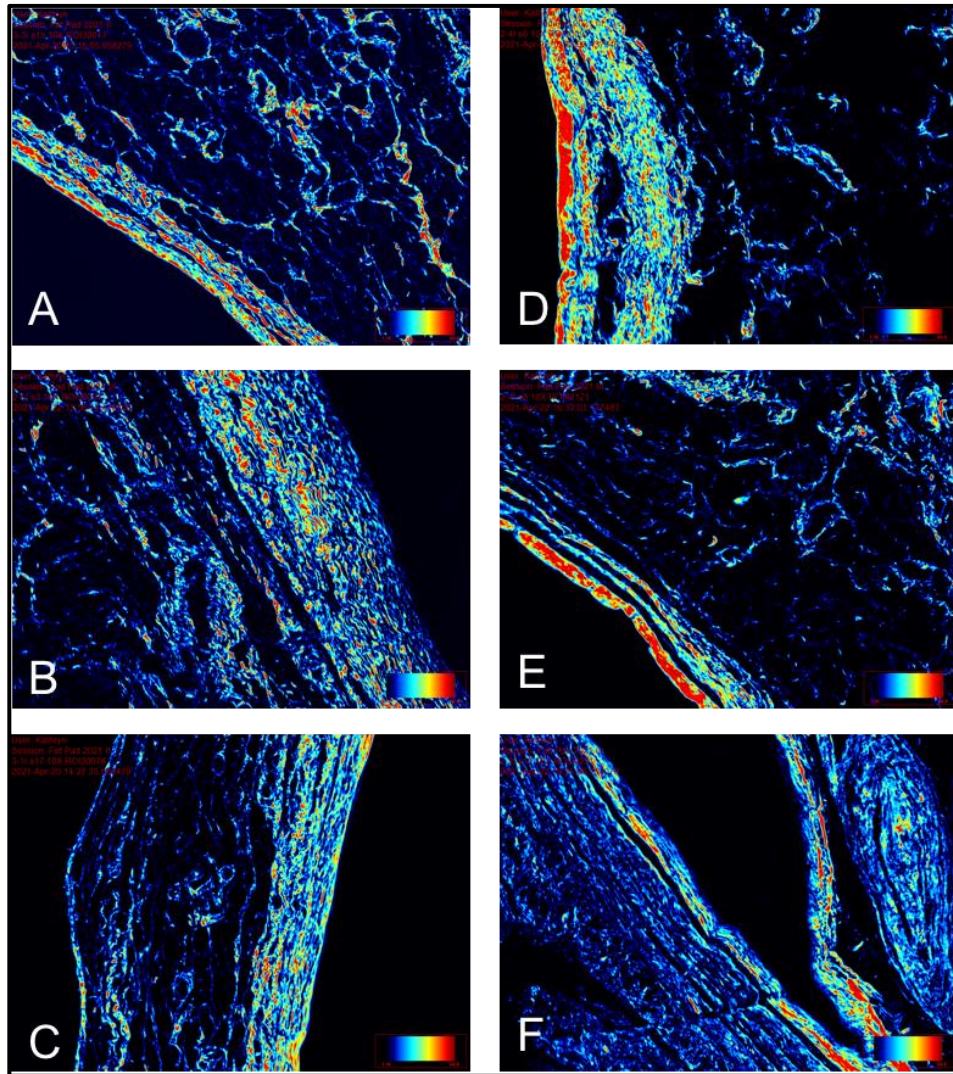


Figure 17. Representative images of paraffin embedded tissue sections of right 4th implant capsule and adjacent fat pad stained with Picrosirius Red, at 10X. Red indicating denser collagen bundling and networks. A-C. Non-radiated. D-F Radiated.

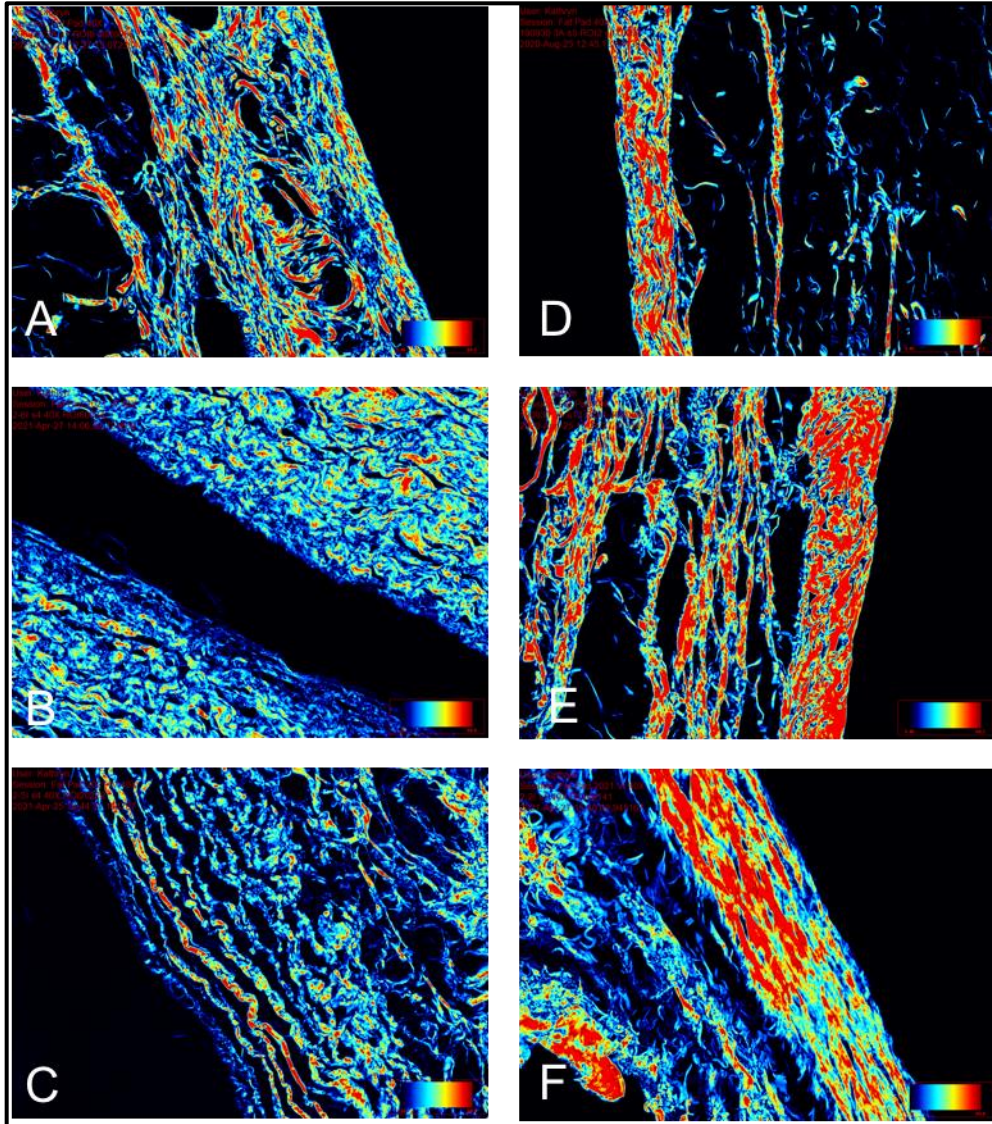


Figure 18. Representative images of paraffin embedded tissue sections of right 4th implant capsule and adjacent fat pad stained with Picrosirius Red, at 40X. Red indicating denser collagen bundling and networks. A-C. Non-radiated. D-F Radiated.

For analysis, the number of red and blue pixels were quantified for each image, and the average pixel count was calculated for the 4 groups; right 4th implant capsule radiated and non-radiated, and left 4th sham surgery fat pad radiated and non-radiated. For both implant capsule groups, tissue section images were from 6 animals. The number of images used for analysis from each animal was variable after excluding images that did not contain capsule. For the sham groups, tissue section images were from 3 non-radiated, and 2 radiated animals. Figure 19 shows the average red and blue pixel count for each group. There was no significant difference in average red pixel count for radiated and non-radiated right 4th implant capsule tissue sections (68993.109 vs 80628.836, $p = 0.34$). The left 4th sham surgery tissue sections trended for more red pixels in the non-radiated group than radiated, but this was not significant ($p = 0.10$). There were similar average blue pixels for both radiated and non-radiated groups.

When the ratio of red to blue pixel count was compared, there was also no difference for radiated and non-radiated right 4th implant capsule tissue sections, with both having a 1:1 ratio of red to blue pixels (Figure 20). As well, the ratio of red to blue pixel count was similar for the left 4th sham surgery groups, at 1:1 for radiated, and slightly more for non-radiated, although not significant. These findings demonstrate similar ratio of red and blue pixels in radiated capsule samples and non-radiated capsules, indicating that the density of collagen bundling is similar.

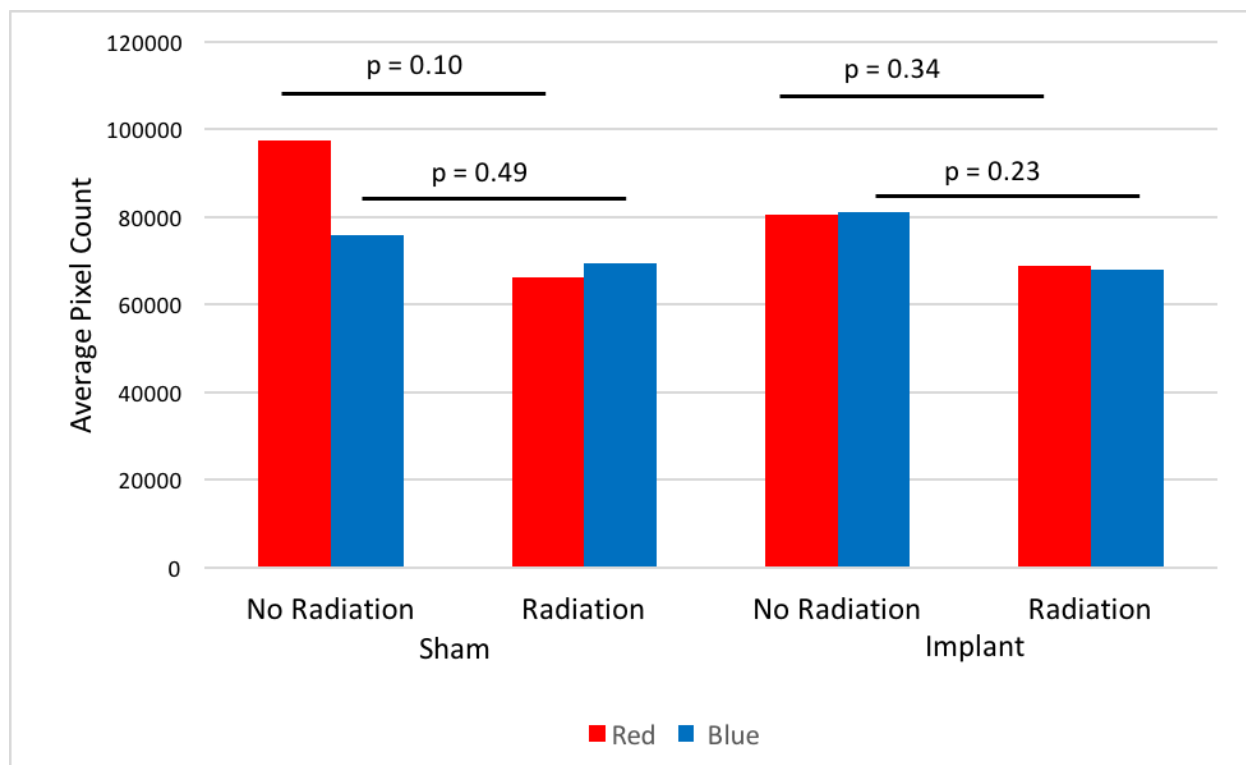


Figure 19. Average red and blue pixel count for picosirius red 40X images of right 4th implant capsule and left 4th sham surgery fat pad for both radiated and non-radiated animals.

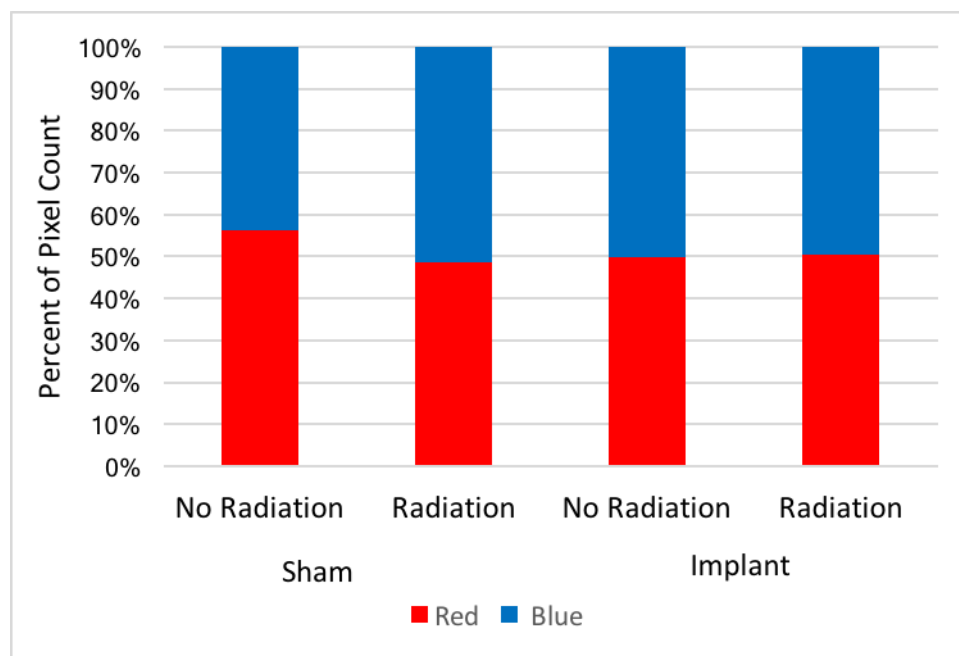


Figure 20. Red and blue pixel count expressed as proportion of total pixel count. Picosirius red 40X images of right 4th implant capsule and left 4th sham surgery fat pad for both radiated and non-radiated animals

4.4 Tissue Assays - Hydroxyproline to Total Protein Assay

Hydroxyproline content in the tissue was measured as a standard measurement of collagen in order to further quantify fibrosis in our tissue samples. The ratio of hydroxyproline to total protein was used to normalize for difference in the amount of tissue in each sample. The ratio of hydroxyproline to total protein for the right 4th implant capsule and fat pad was significantly greater for the radiated group than that of the non-radiated group using Mann Whitney U-test (0.0235 vs 0.0192, $U=3$, $p < 0.05$) (Figure 21). Comparison of the average ratio for first set of radiated animals to the second set of radiated animals found no significant difference between the two groups (0.0236 vs 0.0235, $U=13$, $p=0.857$) indicating both methods of radiation set-up increased collagen content in the tissues (Figure 22). In addition, the average ratio of both radiation experimental sets was significantly higher than the non-radiated group (set 1, $U=1$, $p=0.048$; set 2, $U=2$, $p=0.038$). For the tissue samples taken from the left 4th fat pad sham surgery side, there was no significant difference between the radiated and non-radiated animals (0.0285 vs 0.0302, $U=64$, $p=0.667$) indicating radiation did not increase the collagen content on the left sham surgery side (Figure 23).

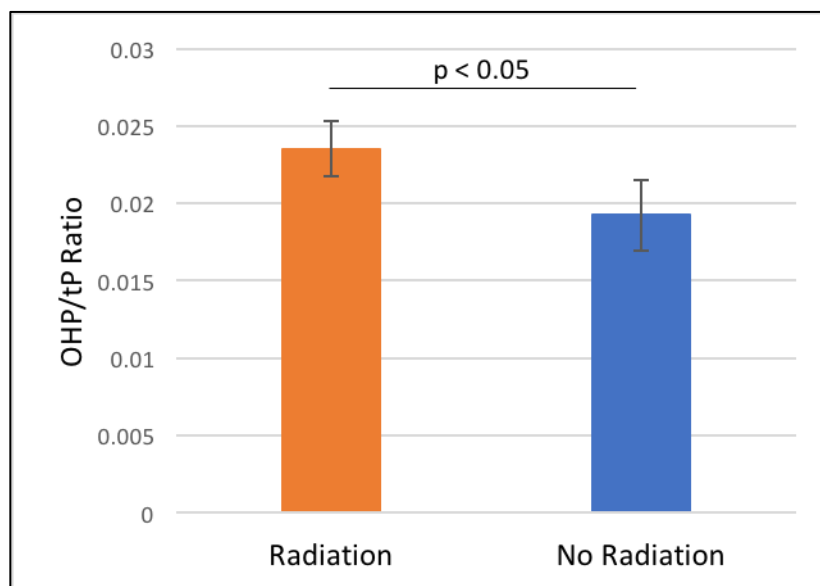


Figure 21. Calculated hydroxyproline (OHP) to total protein (tP) ratio for right 4th implant capsule and fat pad in radiated and non-radiated animals. Twenty-five 10 μ M sections from each animal were used ($n = 7$ radiated, $n = 6$ non-radiated). Six technical replicates were run per sample.

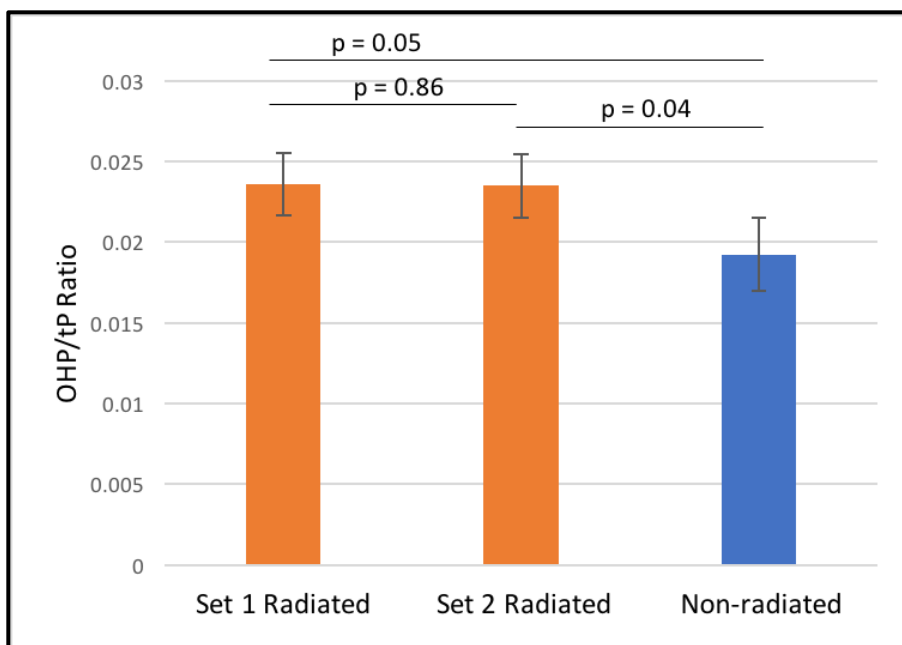


Figure 22. Calculated hydroxyproline (OHP) to total protein (tP) ratio for right 4th implant capsule and fat pad in radiated and non-radiated animals. Set 1 radiated animals ($n = 3$) and set 2 radiated animals using the “ratform” ($n=4$), twenty-five 10uM sections from each animal were used ($n=6$ non-radiated). Six technical replicates were run per sample.

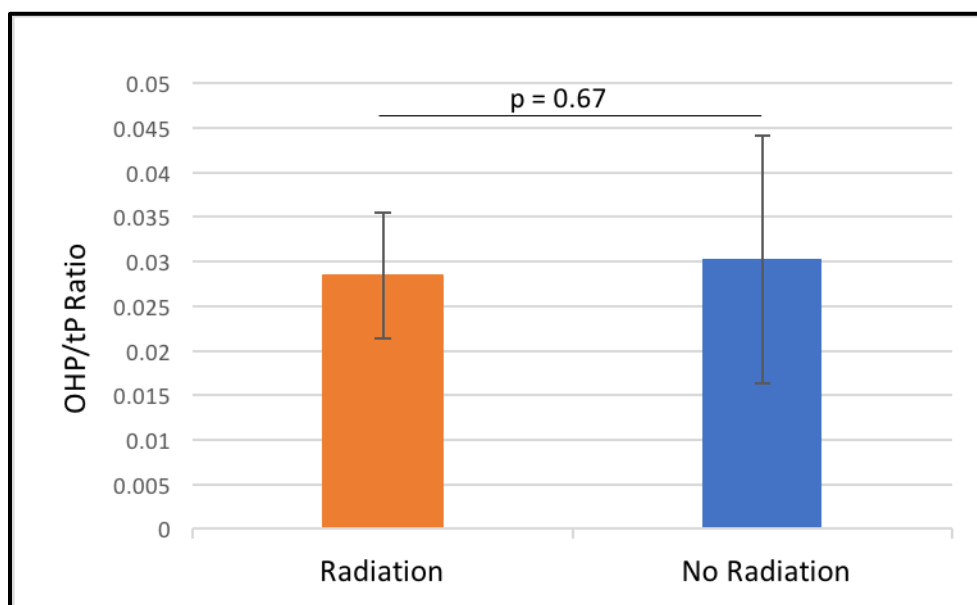


Figure 23. Calculated hydroxyproline (OHP) to total protein (tP) ratio for the left 4th sham surgery fat pad in radiated and non-radiated animals. Twenty-five 10uM sections from two animals in both groups were used (2 non-radiated, 2 radiated). Six technical replicates were run per sample.

5 Discussion

The main objective of this thesis was to establish a unique *in vivo* rodent model of radiation-induced breast implant capsule contracture that replicates both the type of implant and the anatomic positioning used in humans. This animal model is unique in these features compared to other published models. The intention is that it can subsequently be used in future studies to identify potential non-surgical therapies that reduce capsular contracture.

5.1 Objective 1

Modify the previously established rodent model of radiation-induced mammary fat pad fibrosis developed by Truong et al to include a sub-mammary gland silicone prosthesis.

5.1.1 Aim 1

Develop a standard surgical procedure in a rodent model that can be easily replicated involving the implantation of a right 4th sub-mammary fat pad silicone prosthesis.

The surgical protocol developed was easily standardized and the technical skill required to carry it out was minimal. The surgeries were carried out with one main “surgeon” (T. DeLyzer), and one “assistant” (K. Minkhorst). The standardization of the steps allowed for ease of replication and efficiency, minimizing time required to carry out the surgeries. The efficiency increased as the number of surgeries performed increased. The total operative time decreased from approximately 45mins to 25mins by the end of the study.

This model is unique in that, the implants used were supplied by Johnson and Johnson (Mentor) and were exact replicates of implants used in humans. There has been inconsistency in the literature with type of material implanted in previous models. The implants used here consisted of a cohesive silicone gel with a smooth silicone shell and were 2cc in size. Currently, smooth implant devices are the most common choice in reconstruction. Previously, textured devices were available, and some studies have shown a difference in capsule formation between the types of implants, with texturing leading to less contracture, although there is heterogeneity in the literature regarding this⁶¹. The risk of developing a breast implant associated anaplastic large cell lymphoma (BIA-ALCL) has been increasingly recognized, and therefore Health Canada issued a recall in 2019 on macro-textured devices⁶². This has led to smooth devices now being

the implant of preference. In this study, the implants were irrigated prior to implantation with betadine, mimicking the protocol used in human surgery, where implants and surgical pockets are routinely irrigated with povidone-iodine solution prior to implantation. Irrigation of the pocket with povidone-iodine has been shown to decrease the risk of capsular contracture compared to saline irrigation⁶³.

The location of implantation was chosen as sub-mammary fat pad, as the previous work by *Truong et al* found that fibrosis was induced in the fat pad with their radiation technique. This location replicates the sub-mammary position in humans and is unique in current animal models of capsular contracture. Implant capsular contracture risk is less for a partial or full sub-muscular position in humans, with placement below the pectoralis muscle. This is attributed to the movements of the muscle, which contribute to continuous massage of the implant, as well as the muscle providing a protective barrier from bacteria-laden breast tissue⁶¹. In rodents, however, due to the anatomy and size of the muscle, it is not feasible to place the implant sub-pectoralis. The 4th mammary fat pad in the rodent is located just cranial/adjacent to the hind leg in the rat, thus the implant in this position is subject to movement of the hind leg. This is similar to humans where the implant is subject to forces from the upper limb movement and the pectoralis muscle. In addition, the placement at the right 4th mammary fat pad avoids radiation delivery to critical structures such as heart, lungs, and spleen.

This aim was successful in developing a standard surgical procedure for implantation of a right 4th sub-mammary fat pad silicone prosthesis in a rat model that can be easily replicated.

5.1.2 Aim 2

Develop a standard radiation protocol to deliver one-time dose of irradiation to the 4th right mammary fat pad and implant for a total dose of 26Gy.

The radiation delivery was altered from that of *Truong et al* due to the presence of the implant. The field size required adjustment to a larger size to accommodate the implant diameter (3cm vs 1cm), and the photon beam energy was adjusted (6MV vs 100kV). In total, 26Gy was delivered in one dose to the right 4th mammary fat pad and implant. The main goal of a single dose is to maximize the development of capsular contracture while minimizing systemic effects of radiation.

In addition, a single dose simplified the radiation protocol and limited the number of general anaesthetics required for the animals to a maximum of two. In standard breast radiation protocols, the irradiation is delivered with smaller doses in multiple fractions. This is meant to reduce radiation-induced complications while allowing for a higher total dose. This is impractical in an animal model, as it would require multiple treatments and anaesthetics increasing the study time and resources, but also increasing the risk of anaesthetic related complications for the study animals. There were no adverse effects that occurred from the radiation delivery or general anaesthetic in this study. The radiation set-up changed with the second set of animals as the 3D printed “ratform” was created and found to be effective in isolating the fat pad and implant. This made the set-up of the animal easier and also more efficient as the animal could be easily positioned on the rat-form once anesthesia induced. This shortened the time under general anaesthetic by approximately 10mins.

This aim was successful in developing a simple one 26Gy dose radiation protocol that can efficiently be repeated. This was improved by the 3D printed “ratform”. 3D printed shields and boluses is a growing technique in radiation treatment for patients, and can aid in protecting healthy tissues from unwanted radiation⁶⁴. This “ratform” is unique and a new technique in animal studies, with only two other similar techniques found in the literature that used similar devices^{65,66}.

5.1.3 Aim 3

After surgery and delivery of radiation treatment; use established clinical assessments of capsular contracture and radiation fibrosis to evaluate for effect.

The Kumar score at 7-days post-radiation demonstrated a noticeable effect for all right 4th mammary fat pads and implants. The score decreased by week 4 for the animals in the first set of radiation, but increased for the second set. Thus, indicating that the radiation-induced a greater effect for the second set of animals. This increased effect can be attributed to the set-up for these animals, using the 3D printed “ratform”. There was no clinical evidence of radiation effect, or fibrosis, on left 4th mammary fat pad sides (sham surgery). This demonstrates that the radiation delivery technique was effective in blocking of adjacent tissue.

Using the Baker grading scale for capsular contracture, there was a difference between animals that had the implants radiated and those that did not. The radiation technique used induced a noticeable change in the implant capsules, with firmness and decreased mobility. This was greater for the second set of radiated animals (Baker grade 3), demonstrating that the set-up and delivery of radiation was more effective than in the first set.

This aim was successful in the utilization of the Kumar score and Baker grade clinical assessment scales to evaluate the effect of the radiation treatment.

5.1.4 Conclusions and Limitations of Objective 1

In practical terms the goal for this objective was to develop an efficient surgical and radiation protocol, and induce a clinically detectable fibrosis and contracture of the implant capsule without systemic side effects, and ultimately within a reasonable study period. The time from surgery to euthanasia was 8-9 weeks. The actual surgical procedure time reduced with repeated experience. The radiation set-up was improved to make it more efficient, and successfully reduced the amount of time required for general anesthesia. The greatest limitation has been the COVID-19 pandemic. Unfortunately, the pandemic shutdowns lengthened the time between the first set and second set of animals, prolonging the total study period. Other delays were encountered at the outset, with obtaining custom implants from the implant manufacturer, however these custom implants strengthen the utility of the model as they replicate the implants used in humans. The other time limitation was the unit used for radiation delivery, as it is in an area that is used for clinical patient use, we had to organize utilization after-hours, and co-ordinate the surgery to occur 4-weeks prior to when the unit was available. Ultimately, objective 1 was successful.

5.2 Objective 2

To assess for increased fibrosis induced by radiation, of the implant capsules and adjacent mammary fat pads, compared to non-radiated implant capsules and adjacent mammary fat pads.

5.2.1 Aim 1

Use paraffin embedded tissue sections stained for Masson's Trichrome and Picrosirius Red to quantify collagen content and collagen architecture of the right 4th implant capsule and adjacent

mammary fat pad in radiated animals compared to non-radiated. As well as in the left 4th mammary fat pad sham surgery tissue samples.

Qualitatively and quantitatively an increase in blue staining, indicating increased collagen, was seen with Masson's trichrome stained tissue sections of implant capsule of radiated animals compared to non-radiated animals. This was seen independently with both sets of radiation delivery, with significantly more blue staining with both techniques compared to non-radiated animals. The blue staining was similar in the sham surgery fat pad sections from radiated and non-radiated animals, indicating that there was not increased collagen and fibrosis, and adequate shielding of the left side during radiation delivery. These results demonstrate that there was increased collagen content in the radiated implant capsules, indicating increased fibrosis. This is consistent with the clinical results.

Picrosirius red staining with visualization under polarized light demonstrated increasing collagen fibril density when going from blue to red hue. Qualitatively when examining the images of implant capsule sections, an increase in red hue compared to blue was seen. ImageJ software was used to quantify pixel counts in the images for red and blue. There was not a significant difference between radiated and non-radiated implant capsule sections with this method. This could indicate that the orientation and bundling of the fibers is similar in both radiated and non-radiated animals. However, this could also be an error in analysis. The limitation of this analysis was that there was variability in the image acquisition, with some ROI images not taken of the implant capsule. Thus, not capturing the area of interest. These images were excluded from analysis and thus we had variable numbers of images to analyze, with one radiated animal having no usable images. Interestingly, *Moyer and Ehrlich* found that with worsening capsular contracture there was a transition from fine collagen fibers into thicker fibers²². In their study, picrosirius analysis was used to look human implant capsules, and showed fine collagen fibers appearing with green birefringence at the periphery of collagen dense cables showing red birefringence. With greater severity of contracture (Baker 3) they found decreasing, or an absence, of the fine fibers with green birefringence, noting that the collagen fibers not only become thicker but establish into cable-like structures resembling a helical orientation. This pattern of green and red birefringence can be seen in Figure 17 and 18, with the same progression to thicker cables of red birefringence in radiated implant capsules.

This aim was successful in using Masson's trichrome staining for collagen content. The results for the Picosirius red analysis when qualitatively reviewed showed increased density of collagen fibers with radiation, but the quantification was not consistent with this. In future studies, image acquisition will need to be improved in order to ensure proper capture of the region of interest.

5.2.2 Aim 2

Use tissue hydrolysis assays for hydroxyproline and total protein to quantify the amount of collagen in tissue samples of the right 4th implant capsule and adjacent mammary fat pads in radiated animals compared to non-radiated. As well as in the left 4th mammary fat pad sham surgery tissue samples.

Collagen can be quantified by hydroxyproline content since this amino acid is present almost exclusively in collagen⁶⁷. The ratio of hydroxyproline to total protein in the tissue samples was used to control for differences in the amount of tissue in each hydrolysate. This is a unique technique to measure collagen content. The right 4th implant and fat pad radiated tissue samples showed a higher OHP to TP ratio when compared to non-radiated, and this was consistent for both sets of radiation delivery. This indicates increasing collagen content in these samples, consistent with increasing fibrosis. In the sham surgery samples, a difference was not found between radiated and non-radiated samples, indicating no increase in fibrosis and effective blocking during radiation delivery. These results demonstrate that our radiation delivery was successful in inducing fibrosis in a quantifiable manner.

5.2.3 Conclusions and Limitations of Objective 2

Through Masson's trichrome staining, picosirius red staining, and hydroxyproline tissue assays, a measurable increase in fibrosis was noted in radiated implant capsules correlating with the clinical results of our first objective. Both Masson's trichrome analysis and OHP to TP analysis showed increased collagen content in radiated implant capsule tissue sections. Picosirius red analysis demonstrated qualitatively an increase in fibril thickness indicating denser collagen bundling in radiated capsules. The quantitative analysis did not show a difference between the ratio of red and blue pixels in radiated samples, possibly indicating no difference in collagen bundling. However, this is more likely a limitation of image sampling.

Together with Objective 1, the results of Objective 2 demonstrate that this model was successful in inducing a measurable and quantifiable increase in contracture of the implant capsules. In conclusion, this thesis describes a novel and effective rodent model of radiation-induced capsular contracture that can be used in future studies.

6 Impact and Future Directions

Implant-based techniques remain the most common form of post-oncologic breast reconstruction. Radiation-induced capsular contracture is the greatest challenge of implant-based techniques, remaining a difficult and recurrent problem. Unfortunately, even after surgical treatment with capsulectomy and implant replacement, patients can continue to have problems with further recurrences. This exposes the patient to additional risks of further surgery and devastating psychological impact. Roberts et al. examined the rates of re-operation in post-mastectomy breast reconstruction in Ontario between 2002-2008 and found that for implant-based reconstructions, patients on average experienced one unanticipated major re-operation⁶⁸. This would mean 2, 854 additional unanticipated surgeries in the province over the study period. The most common reason (77%) cited for all unanticipated major re-operations was “breast mound revision”, and for implant reconstructions, this would largely mean correction of capsular contracture amongst other reasons. In today’s health care climate, the importance of reducing the number of surgeries, and therefore the cost of treatment and the cost to the health care system, is imperative. Recently there has been a surge of interest in understanding the patho-etiology of radiation-induced capsular contracture. There is a great need for the development of evidence-based, non-surgical, preventative and treatment options. In this thesis, a novel laboratory animal model has been developed by which we can better understand radiation-induced capsular contracture and test potential non-surgical therapeutic interventions.

Currently, there are limited treatments for radiation-induced fibrosis. Vitamin E, or alpha-tocopherol, is a potent anti-inflammatory and antioxidant. Pentoxifylline has also been used in prevention of radiation injury. The use of the two drugs in combination has been used in breast oncology, and has been shown to reverse late radiotherapy skin damage. However, long course of treatment is required and can have “bounce back” affect with cessation limiting their utilization⁶⁹.

6.1 Hyaluronan

Hyaluronan is ubiquitous in the extracellular matrix and is fundamental to maintaining normal tissue homeostasis and regulating fibroblast function^{70,71}. With tissue stress and oxidative injury, the native form is fragmented into pro-inflammatory lower molecular weight oligosaccharides

and is one of the earliest detectable changes to tissue injury. Hyaluronan is the major extracellular ligand for RHAMM (receptor for hyaluronan mediated motility) which is a TGF β -1 target gene and key regulator for directing mesenchymal progenitor cells into myofibroblasts and dermal fibroblast lineages^{72,73}. RHAMM is transiently expressed in injured tissues but is normally low in homeostatic tissues⁷⁴. The silencing of RHAMM reduces injury-induced fibrosis and supports adipogenesis; therefore, targeting RHAMM is a potential strategy for controlling radiation-induced fibrosis^{72,75-78}. Previous studies have demonstrated a local increase in hyaluronan within breast capsular tissue⁷⁹. Serum hyaluronan levels were elevated in patients with capsular contracture and increasing levels were correlated with higher grades of contracture^{80,81}.

The Turley lab has developed injectable function-blocking peptides against RHAMM, HA binding peptides, that blunt fibrotic changes in both a mouse model of cutaneous scleroderma and rat model of radiation-induced mammary fat pad fibrosis^{57,82}. The RHAMM peptide mimetics bind small hyaluronan fragments produced during tissue injury (<10 kDa). These competitively remove pro-inflammatory hyaluronan fragments and effectively blunt RHAMM-directed signaling of fibrogenesis^{77,78}. Several of the RHAMM peptide mimetics, including NPI-102, have previously been shown to reduce TGF β -1-regulated fibrosis and to promote adipocyte differentiation of bone marrow mesenchymal stem cells in culture⁷⁷. NPI-102 has a limited half-life in inflamed tissues and was stabilized by N and C-terminal acetylation to increase its serum half-life to greater than 24 hours, creating peptide NPI-110. In the bleomycin-induced mouse model of scleroderma, NPI-110 was shown to significantly decrease collagen 1 and collagen 3 expression, as well as the collagen 1:3 ratio, which is characteristic of fibrosis⁸². The peptide also decreased TGF β -1 activity as evidenced by immunostaining, and reduced dermal collagen deposition and bundling, visualized by picrosirius red staining and polarized microscopy⁸².

The peptides used in these prior studies have since been further optimized with cyclization or ‘stapling’ to enhance their binding affinity and to increase peptide stability. These novel stapled peptides are predicted to have more potent anti-fibrotic properties. These peptides have the potential to make an impactful difference as a non-surgical option available to women with radiation-induced breast capsular contracture. In future studies, this animal model can be used to test the efficacy of these peptides in preventing or reducing the severity of capsular contracture.

References

1. Brenner, D. R. *et al.* Projected estimates of cancer in Canada in 2020. *CMAJ* **192**, E199–E205 (2020).
2. res-cancerstatistics-canadiancancerstatistics-2019-en.pdf.
3. Albornoz, C. R. *et al.* A paradigm shift in U.S. Breast reconstruction: increasing implant rates. *Plast Reconstr Surg* **131**, 15–23 (2013).
4. Cemal, Y. *et al.* A paradigm shift in U.S. breast reconstruction: Part 2. The influence of changing mastectomy patterns on reconstructive rate and method. *Plast Reconstr Surg* **131**, 320e–326e (2013).
5. Wazir, U. & Mokbel, K. The evolving role of pre-pectoral ADM-assisted implant-based immediate breast reconstruction following skin-sparing mastectomy. *Am J Surg* **216**, 639–640 (2018).
6. Lin, A. M. *et al.* Abstract 70: The Impact of Post-Mastectomy Radiation Therapy on Permanent Implants in Direct-to-Implant Breast Reconstruction versus Tissue Expanders in Two-Stage Breast Reconstruction. *Plast Reconstr Surg Glob Open* **6**, 55–56 (2018).
7. Recht, A. *et al.* Postmastectomy Radiotherapy: An American Society of Clinical Oncology, American Society for Radiation Oncology, and Society of Surgical Oncology Focused Guideline Update. *Pract Radiat Oncol* **6**, e219–e234 (2016).
8. Lao, N. *et al.* Redefining postmastectomy radiation contouring in the era of immediate breast reconstruction: An accurate assessment of local recurrence risk. *Clin Transl Radiat Oncol* **29**, 33–39 (2021).

9. Recht, A. *et al.* Postmastectomy Radiotherapy: An American Society of Clinical Oncology, American Society for Radiation Oncology, and Society of Surgical Oncology Focused Guideline Update. *Ann Surg Oncol* **24**, 38–51 (2017).
10. Pu, Y., Mao, T.-C., Zhang, Y.-M., Wang, S. & Fan, D.-L. The role of postmastectomy radiation therapy in patients with immediate prosthetic breast reconstruction: A meta-analysis. *Medicine* **97**, e9548 (2018).
11. Cronin, P., Sacchini, V. & Marti, J. Oncologic Principles for Breast Reconstruction: Indications and Limits. in 223–231 (2019). doi:10.1007/978-3-319-62927-8_17.
12. Yan, C. *et al.* The Timing of Breast Irradiation in Two-Stage Expander/Implant Breast Reconstruction. *Breast J* **22**, 322–329 (2016).
13. Effect of radiotherapy after breast-conserving surgery on 10-year recurrence and 15-year breast cancer death: meta-analysis of individual patient data for 10 801 women in 17 randomised trials. *Lancet* **378**, 1707–1716 (2011).
14. 2020 Plastic Surgery Statistics Report. *PLASTIC SURGERY* 26 (2020).
15. Serritzlev, M. S., Lorentzen, A. K., Matthiessen, L. W. & Hölmich, L. R. Capsular contracture in patients with prior breast augmentation undergoing breast conserving therapy and irradiation. *J Plast Surg Hand Surg* **54**, 225–232 (2020).
16. NCCN Breast 2020.pdf.
17. Handel, N., Cordray, T., Gutierrez, J. & Jensen, J. A. A long-term study of outcomes, complications, and patient satisfaction with breast implants. *Plast Reconstr Surg* **117**, 757–767; discussion 768-772 (2006).
18. Cunningham, B. The Mentor Core Study on Silicone MemoryGel Breast Implants. *Plast Reconstr Surg* **120**, 19S-29S (2007).

19. Cunningham, B. The Mentor Study on Contour Profile Gel Silicone MemoryGel Breast Implants. *Plast Reconstr Surg* **120**, 33S-39S (2007).
20. Spear, S. L., Murphy, D. K., & Allergan Silicone Breast Implant U.S. Core Clinical Study Group. Natrelle round silicone breast implants: Core Study results at 10 years. *Plast Reconstr Surg* **133**, 1354–1361 (2014).
21. Araco, A., Caruso, R., Araco, F., Overton, J. & Gravante, G. Capsular contractures: a systematic review. *Plast Reconstr Surg* **124**, 1808–1819 (2009).
22. Moyer, K. E. & Ehrlich, H. P. Capsular Contracture after Breast Reconstruction: Collagen Fiber Orientation and Organization. *Plastic and Reconstructive Surgery* **131**, 680–685 (2013).
23. Bui, J. M. *et al.* Histological characterization of human breast implant capsules. *Aesthetic Plast Surg* **39**, 306–315 (2015).
24. Avery, D. *et al.* Extracellular matrix directs phenotypic heterogeneity of activated fibroblasts. *Matrix Biol* **67**, 90–106 (2018).
25. Juillerat-Jeanneret, L., Tafelmeyer, P. & Golshayan, D. Fibroblast activation protein- α in fibrogenic disorders and cancer: more than a prolyl-specific peptidase? *Expert Opin Ther Targets* **21**, 977–991 (2017).
26. Darby, I. A., Laverdet, B., Bonté, F. & Desmoulière, A. Fibroblasts and myofibroblasts in wound healing. *Clin Cosmet Investig Dermatol* **7**, 301–311 (2014).
27. Ricci, J. A. *et al.* A meta-analysis of implant-based breast reconstruction and timing of adjuvant radiation therapy. *J Surg Res* **218**, 108–116 (2017).

28. El-Diwany, M., Giot, J.-P., Hébert, M.-J. & Danino, A. M. Delaying implant-based mammary reconstruction after radiotherapy does not decrease capsular contracture: An in vitro study. *J Plast Reconstr Aesthet Surg* **70**, 1210–1217 (2017).
29. Adams, W. P. Capsular contracture: what is it? What causes it? How can it be prevented and managed? *Clin Plast Surg* **36**, 119–126, vii (2009).
30. Adams, W. P., Rios, J. L. & Smith, S. J. Enhancing patient outcomes in aesthetic and reconstructive breast surgery using triple antibiotic breast irrigation: six-year prospective clinical study. *Plast Reconstr Surg* **118**, 46S-52S (2006).
31. Yalanis, G. C., Liu, E.-W. & Cheng, H.-T. Efficacy and Safety of Povidone-Iodine Irrigation in Reducing the Risk of Capsular Contracture in Aesthetic Breast Augmentation: A Systematic Review and Meta-Analysis. *Plast Reconstr Surg* **136**, 687–698 (2015).
32. Wang, Y., Tian, J. & Liu, J. Suppressive Effect of Leukotriene Antagonists on Capsular Contracture in Patients Who Underwent Breast Surgery with Prosthesis: A Meta-Analysis. *Plast Reconstr Surg* **145**, 901–911 (2020).
33. Barcellos-Hoff, M. H. The radiobiology of TGF β . *Seminars in Cancer Biology* (2022) doi:10.1016/j.semcancer.2022.02.001.
34. Straub, J. M. *et al.* Radiation-induced fibrosis: mechanisms and implications for therapy. *J Cancer Res Clin Oncol* **141**, 1985–1994 (2015).
35. Barcellos-Hoff, M. H. & Mao, J.-H. HZE Radiation Non-Targeted Effects on the Microenvironment That Mediate Mammary Carcinogenesis. *Front Oncol* **6**, 57 (2016).
36. Chargari, C. *et al.* Complications of thoracic radiotherapy. *Presse Med* **42**, e342-351 (2013).

37. Martin, M. TGF- α 1 AND RADIATION FIBROSIS: A MASTER SWITCH AND A SPECIFIC THERAPEUTIC TARGET? **47**, 14 (2000).
38. Katzel, E. B. *et al.* The Impact of Smad3 Loss of Function on TGF- β Signaling and Radiation-Induced Capsular Contracture: *Plastic and Reconstructive Surgery* **127**, 2263–2269 (2011).
39. Baker, J. J., Owsley, J. J. & Peterson, R. Augmentation mammoplasty. *Symposium on Aesthetic Surgery of the Breast* 256–263 (1978).
40. Spear, S. L. & Baker, J. L. Classification of capsular contracture after prosthetic breast reconstruction. *Plast Reconstr Surg* **96**, 1119–1123; discussion 1124 (1995).
41. Jacombs, A. *et al.* Prevention of biofilm-induced capsular contracture with antibiotic-impregnated mesh in a porcine model. *Aesthet Surg J* **32**, 886–891 (2012).
42. Jacombs, A. *et al.* In vitro and in vivo investigation of the influence of implant surface on the formation of bacterial biofilm in mammary implants. *Plast Reconstr Surg* **133**, 471e–480e (2014).
43. Marques, M. *et al.* Animal model of implant capsular contracture: effects of chitosan. *Aesthet Surg J* **31**, 540–550 (2011).
44. Marques, M. *et al.* Effects of coagulase-negative staphylococci and fibrin on breast capsule formation in a rabbit model. *Aesthet Surg J* **31**, 420–428 (2011).
45. Shah, Z., Lehman, J. A. & Tan, J. Does infection play a role in breast capsular contracture? *Plast Reconstr Surg* **68**, 34–42 (1981).
46. Kumar, S. *et al.* Radiation-induced skin injury in the animal model of scleroderma: implications for post-radiotherapy fibrosis. *Radiat Oncol* **3**, 40 (2008).

47. Rodgers, K. E. *et al.* Development of a guinea pig cutaneous radiation injury model using low penetrating X-rays. *Int J Radiat Biol* **92**, 434–443 (2016).
48. Vieira, V. J. *et al.* Capsular Contracture In Silicone Breast Implants: Insights From Rat Models. *An. Acad. Bras. Ciênc.* **88**, 1459–1470 (2016).
49. Takikawa, M. *et al.* New model of radiation-induced skin ulcer in rats. *Journal of Plastic Surgery and Hand Surgery* **45**, 258–262 (2011).
50. Wright, M. A. *et al.* Periprosthetic Capsule Formation and Contracture in a Rodent Model of Implant-Based Breast Reconstruction With Delayed Radiotherapy. *Ann Plast Surg* **82**, S264–S270 (2019).
51. Diehm, Y. F. *et al.* The Collagenase of the Bacterium *Clostridium histolyticum* in the Treatment of Irradiation-Induced Capsular Contracture. *Aesth Plast Surg* **43**, 836–844 (2019).
52. Katzel, E. B. *et al.* A Novel Animal Model for Studying Silicone Gel-Related Capsular Contracture: *Plastic and Reconstructive Surgery* **126**, 1483–1491 (2010).
53. Diehm, Y. F. *et al.* The Treatment of Capsular Contracture Around Breast Implants Induced by Fractionated Irradiation: The Collagenase of the Bacterium *Clostridium Histolyticum* as a Novel Therapeutic Approach. *Aesth Plast Surg* **45**, 1273–1281 (2021).
54. Eltze, E. *et al.* Radiation-induced capsule tissue reactions around textured breast implants in a rat model. *The Breast* **15**, 331–338 (2006).
55. Erpolat, O. P. *et al.* Angiotensin-Converting Enzyme Inhibitor Reduces Radiation-Induced Periprosthetic Capsular Fibrosis. *Journal of Surgical Research* **263**, 167–175 (2021).
56. Kim, J. B. *et al.* A murine model of radiation-induced capsule-tissue reactions around smooth silicone implants. *Journal of Plastic Surgery and Hand Surgery* **52**, 217–224 (2018).

57. Truong, J. L. *et al.* Creating a Favorable Microenvironment for Fat Grafting in a Novel Model of Radiation-Induced Mammary Fat Pad Fibrosis. *Plast Reconstr Surg* **145**, 116–126 (2020).
58. Charan, J. & Kantharia, N. D. How to calculate sample size in animal studies? *Journal of Pharmacology and Pharmacotherapeutics* **4**, 303–306 (2013).
59. P, S. The Laboratory Rat: Relating Its Age With Human's. *International journal of preventive medicine* **4**, (2013).
60. Rich, L. & Whittaker, P. COLLAGEN AND PICROSIRIUS RED STAINING: A POLARIZED LIGHT ASSESSMENT OF FIBRILLAR HUE AND SPATIAL DISTRIBUTION. **8** (2005).
61. Bachour, Y. *et al.* Risk factors for developing capsular contracture in women after breast implant surgery: A systematic review of the literature. *J Plast Reconstr Aesthet Surg* **71**, e29–e48 (2018).
62. Canada, H. Breast implants risks. <https://www.canada.ca/en/health-canada/services/drugs-medical-devices/breast-implants/risks.html> (2020).
63. Awad, A. N., Heiman, A. J. & Patel, A. Implants and Breast Pocket Irrigation: Outcomes of Antibiotic, Antiseptic, and Saline Irrigation. *Aesthet Surg J* **42**, NP102–NP111 (2022).
64. Asfia, A., Novak, J. I., Mohammed, M. I., Rolfe, B. & Kron, T. A review of 3D printed patient specific immobilisation devices in radiotherapy. *Physics and Imaging in Radiation Oncology* **13**, 30–35 (2020).
65. Steinmetz, A. *et al.* Design of a 3D Printed Immobilization Device for Radiation Therapy of Experimental Tumors in Mice. *International Journal of Radiation Oncology, Biology, Physics* **99**, E618 (2017).

66. McCarroll, R. E. *et al.* 3D-Printed Small-Animal Immobilizer for Use in Preclinical Radiotherapy. *Journal of the American Association for Laboratory Animal Science* **54**, 545–548 (2015).
67. Cissell, D. D., Link, J. M., Hu, J. C. & Athanasiou, K. A. A Modified Hydroxyproline Assay Based on Hydrochloric Acid in Ehrlich's Solution Accurately Measures Tissue Collagen Content. *Tissue Eng Part C Methods* **23**, 243–250 (2017).
68. Roberts, A., Baxter, N., Camacho, X., Lau, C. & Zhong, T. Once is Rarely Enough: A Population-Based Study of Reoperations after Postmastectomy Breast Reconstruction. *Ann Surg Oncol* **22**, 3302–3307 (2015).
69. Patel, V. & McGurk, M. Use of pentoxifylline and tocopherol in radiation-induced fibrosis and fibroatrophy. *British Journal of Oral and Maxillofacial Surgery* **55**, 235–241 (2017).
70. Bollyky, P. L., Bogdani, M., Bollyky, J. B., Hull, R. L. & Wight, T. N. The role of hyaluronan and the extracellular matrix in islet inflammation and immune regulation. *Curr Diab Rep* **12**, 471–480 (2012).
71. de la Motte, C. A. Hyaluronan in intestinal homeostasis and inflammation: implications for fibrosis. *Am J Physiol Gastrointest Liver Physiol* **301**, G945-949 (2011).
72. Tolg, C. *et al.* Rhamm^{-/-} fibroblasts are defective in CD44-mediated ERK1,2 mitogenic signaling, leading to defective skin wound repair. *J Cell Biol* **175**, 1017–1028 (2006).
73. Samuel, S. K. *et al.* TGF-beta 1 stimulation of cell locomotion utilizes the hyaluronan receptor RHAMM and hyaluronan. *J Cell Biol* **123**, 749–758 (1993).

74. Misra, S., Hascall, V. C., Markwald, R. R. & Ghatak, S. Interactions between Hyaluronan and Its Receptors (CD44, RHAMM) Regulate the Activities of Inflammation and Cancer. *Front Immunol* **6**, 201 (2015).
75. Zaman, A. *et al.* Expression and role of the hyaluronan receptor RHAMM in inflammation after bleomycin injury. *Am J Respir Cell Mol Biol* **33**, 447–454 (2005).
76. Tolg, C., Telmer, P. & Turley, E. Specific sizes of hyaluronan oligosaccharides stimulate fibroblast migration and excisional wound repair. *PLoS One* **9**, e88479 (2014).
77. Bahrami, S. B. *et al.* Receptor for hyaluronan mediated motility (RHAMM/HMMR) is a novel target for promoting subcutaneous adipogenesis. *Integr Biol (Camb)* **9**, 223–237 (2017).
78. Liu, X.-F. *et al.* ANKRD26 and its interacting partners TRIO, GPS2, HMMR and DIPA regulate adipogenesis in 3T3-L1 cells. *PLoS One* **7**, e38130 (2012).
79. Wells, A. F., Daniels, S., Gunasekaran, S. & Wells, K. E. Local increase in hyaluronic acid and interleukin-2 in the capsules surrounding silicone breast implants. *Ann Plast Surg* **33**, 1–5 (1994).
80. Prantl, L., Pöppl, N., Horvat, N., Heine, N. & Eisenmann-Klein, M. Serologic and histologic findings in patients with capsular contracture after breast augmentation with smooth silicone gel implants: is serum hyaluronan a potential predictor? *Aesthetic Plast Surg* **29**, 510–518 (2005).
81. Ulrich, D., Lichtenegger, F., Eblenkamp, M., Repper, D. & Pallua, N. Matrix metalloproteinases, tissue inhibitors of metalloproteinases, aminoterminal propeptide of procollagen type III, and hyaluronan in sera and tissue of patients with capsular contracture after augmentation with Trilucent breast implants. *Plast Reconstr Surg* **114**, 229–236 (2004).

82. Wu, K. Y. *et al.* Function-Blocking RHAMM Peptides Attenuate Fibrosis and Promote Antifibrotic Adipokines in a Bleomycin-Induced Murine Model of Systemic Sclerosis. *J Invest Dermatol* **141**, 1482-1492.e4 (2021).

TANYA De LYZER, MD, FRCSC

Academic Appointments

Sept 2017 – present Assistant Professor, Department of Surgery, Division of Plastic and Reconstructive Surgery, Schulich School of Medicine and Dentistry, Western University Canada

Clinical Appointments

Sept 2017 – present Plastic Surgeon, London Health Sciences Centre and St. Joseph's Health Care London, Department of Surgery, Division of Plastic and Reconstructive Surgery

Sept 2016 – Nov 2016 Locum Plastic Surgeon
Stratford General Hospital, Stratford Ontario

Post-Graduate Training

Dec 2016 – Feb 2017 Total Burn Care and Complex Wound Reconstruction
Ross Tilley Burn Centre, University of Toronto

2015 – 2016 Breast Reconstruction Fellowship
Toronto General Hospital and Women's College Hospital, University of Toronto

2009 – 2015 Plastic and Reconstructive Surgery Residency
Schulich School of Medicine and Dentistry, Western University Canada

Education

2005 – 2009 Doctor of Medicine
Schulich School of Medicine and Dentistry, Western University Canada

2001 – 2005 Cellular and Molecular Biology, Honours Bachelor of Science (with Distinction)
University of Calgary

Peer Reviewed Grants

1. Lawson Health Research Institute, Lawson Internal Research Fund. Novel peptide for attenuating radiotherapy and implant capsular contractures in breast cancer patients. Principal Investigator. Funding award: \$15 000. Jan 2020 – Dec 2022.

2. Department of Surgery Internal Research Fund, Western University. The Effect of Stapled Function-Blocking RHAMM Peptides in Attenuating the Development of Radiation-Induced Breast Capsular Contracture. Primary Applicant. Funding award: \$20,000. Dec 1 2017 – Nov 30 2019.
3. Competency-based Medical Education Innovation Fund, Western University. Developing an assessment tool for on-call experiences in surgical education. Co – Applicant. Funding Award: \$1500.

Published Articles

1. Lao N, Brackstone M, Formenti SC, Doherty C, Perera F, Chow R, **DeLyzer T**, Grant A, Boldt G, Lock M. Redefining postmastectomy radiation contouring in the era of immediate breast reconstruction: An accurate assessment of local recurrence risk. *Clin Transl Radiat Oncol*, 2021 Jul; 29: 33-39, **Coauthor**, DOI: 10.1016/j.ctro.2021.05.002.
2. Chambers SB, Garland K, Dai C, **DeLyzer T**. Adherence of Burn Outpatient Clinic Referrals to ABA Criteria in a Tertiary Centre: Creating Unnecessary Referrals? *J Burn Care Res*. Online ahead of print. 2021 Jun 17, **Senior Responsible Author**, DOI: 10.1093/jbcr/irab117.
3. S Fan, H Chen, A Grant, **T DeLyzer**. Outcomes of immediate alloplastic breast reconstruction in patients receiving post-mastectomy radiotherapy. *Plastic Surgery*, 2020 Jun 14, **Senior Responsible Author**. Accepted/In Press.
4. Truong JL, Liu M, Tolg C, Barr M, Dai C, Raissi TC, Wong E, **DeLyzer T**, Yazdani A, Turley EA. Creating a Favorable Microenvironment for Fat Grafting in a Novel Model of Radiation-Induced Mammary Fat Pad Fibrosis. *Plast Reconstr Surg*, 2020 Jan; 145 (1): 116-126, **Coauthor**, DOI: 10.1097/PRS.00000000000006344.
5. Tan M, Isaranuwachai W, **DeLyzer T**, Butler K, Hofer SOP, O'Neill AC, and Zhong T. A cost-effectiveness analysis of DIEP versus free MS-TRAM flap for microsurgical breast reconstruction. *Journal of Surgical Oncology*, 2019 Mar 5; 119 (3): 388-396, **Coauthor**, DOI: 10.1002/jso.25325.

Published Abstracts

1. Wu K, Kim S, Turley E, Yazdani A, **DeLyzer T**. Characterizing primary fibroblasts in breast capsular contracture formation. *Plastic Surgery*; 2018. p. 173.
2. Wu K, Kim S, Turley E, Yazdani A, **DeLyzer T**. Effect of function-blocking RHAMM peptides on fibrosis in a bleomycin-induced scleroderma mouse model. *Plastic Surgery*; 2018. p. 173.